Generalized impulse approximation for relativistic proton scattering

J. A. Tjon
Institute for Theoretical Physics, University of Utrecht, 3508 TA Utrecht, The Netherlands

S. J. Wallace
Department of Physics and Astronomy, University of Maryland, College Park, Maryland 20742
(Received 13 February 1987)

A complete set of Lorentz invariant nucleon-nucleon amplitudes, based on a meson-exchange model and on-mass-shell kinematics, is used to construct the impulse approximation optical potential for use in the Dirac equation. Relativistic nuclear densities are also used in the construction. No free parameters enter. The analysis provides a dynamical basis for the virtual pair couplings which are implicit in the Dirac equation for proton-nucleus scattering. A momentum space potential and a localized potential suitable for coordinate space analysis are developed. Initial numerical calculations are presented for proton scattering by ^{40}Ca at 200, 500, and 800 MeV. The generalized impulse approximation provides a successful description of the elastic scattering data for these cases. Low energy results are improved substantially in comparison with the original form of Dirac impulse approximation based on using five Fermi amplitudes to represent nucleon-nucleon scattering.

I. INTRODUCTION

Several years ago, an impulse approximation was suggested in which the optical potential in the Dirac equation is calculated from nucleon-nucleon (NN) scattering data and the nuclear density.[1] No fitting parameters are used in the impulse approximation. However, the general character of the Dirac optical potential reproduces the main features found by fitting phenomenologically the proton-nucleus cross section and analyzing power using the Dirac equation. The impulse approximation in its original form, which is referred to as IA1 in this paper, replaced the 12 fitting parameters of Dirac phenomenology.[2] IA1 also provided an explanation of the large scalar and vector potentials in terms of the relativistic NN amplitudes. Moreover, the experimental data for scattering of 500 MeV protons by ^{40}Ca, particularly the spin observables, were much better described by the Dirac impulse approximation[3,4] than by the traditional Schrödinger impulse approximation.[5] Further analyses[6,7] showed that IA1 provided superior descriptions of most proton elastic scattering data above about 300 MeV. However, it was also found that IA1 predicted overly large scalar and vector potentials at lower proton energies.

The essential difference between Schrödinger and Dirac impulse approximation calculations was identified by Hynes *et al.*[8] to be the implicit incorporation of virtual $N\bar{N}$ pair effects in the Dirac approach. When large scalar and vector potentials are used in the Dirac equation, significant virtual part contributions arise in low momentum transfer processes such as elastic proton scattering. Due to the diffractive nature of elastic scattering, these effects become quite prominent in the predictions of spin observables. However, the specific manner in which the virtual pair effects are predicted by the IA1 approach is questionable. The critical point is that one needs to know the coupling potential connecting positive-energy and negative-energy basis states of the free Dirac equation, the $+$ to $-$ coupling. Experimental data for NN scattering fix the matrix elements between positive-energy basis states, the $+$ to $+$ coupling, but a model or assumption is needed to predict the $+$ to $-$ coupling. IA1 is based on using five Lorentz invariant NN amplitudes[9] with Dirac structure assumed to be given by the standard Fermi covariants: S, V, T, A, and P. Thus the questionable assumption of IA1 is the use of just the Fermi covariants to extend the positive-energy NN data to the full Dirac space of two nucleons.

Fermi covariants are natural from the point of view of meson exchange models of the NN interaction,[10] and they do provide a definite prediction for the Dirac optical potential. However, other choices for the representation of the Lorentz invariant amplitudes cannot be excluded.[11] Other representations generally predict different $+$ to $-$ couplings even when the $+$ to $+$ couplings are held fixed. In principle, one needs a complete set of NN amplitudes on the Dirac space of two nucleons in order to construct unambiguously the Dirac optical potential. Physical NN data are insufficient since they fix the amplitudes in just one sector of the Dirac space, namely when initial and final states are positive energy. Amplitudes in the remaining sectors involving negative-energy states can only be specified in a dynamical model. Since it is precisely these latter amplitudes which control virtual-pair couplings, it is essential to adopt a dynamical model for the NN amplitudes to have a well-founded approach.

Perhaps the best example of the type of ambiguity which can arise is provided by the choice of pseudovector πN coupling versus the choice of pseudoscalar πN coupling.[12] The two are indistinguishable in positive-energy matrix elements (on mass shell), but they provide radically different predictions for the $+$ to $-$ coupling. IA1 naturally embeds pseudoscalar coupling due to the assumption of Fermi covariants and this has been shown to

cause overly large scalar and vector potentials at low proton energy.[12] A related difficulty is overly large virtual-pair contributions to proton-nucleus scattering at low energy. A similar situation exists for NN scattering where meson theoretical analyses[13] indicate a need for pair suppression. This is obtained most simply by adopting pseudovector πN coupling. The need for pair suppression also arises for proton-nucleus scattering. Therefore it is very desirable to incorporate pseudovector πN coupling in the NN amplitudes to remove the most obvious flaw of the IA1 impulse approximation.

A provisional improvement over the IA1 assumption is to adopt a simple five-term representation of the NN amplitudes which forces the one-pion exchange contribution to be pseudovector.[12,14] Essentially one replaces the pseudoscalar covariant with a pseudovector one. It is important to realize that this assumption does not remove the essential ambiguity of extending the NN amplitude defined on positive-energy states into an operator for the full Dirac space. References 12 and 14 present inequivalent ways of replacing the pseudoscalar covariant by a pseudovector one. In principle, the ambiguity which one encounters can only be removed by use of a dynamical model for the NN amplitude on the full Dirac space.

The problem of constructing complete sets of Lorentz invariant NN amplitudes has been addressed in some recent papers.[15-17] There are two parts to the problem. First, one needs a complete set of kinematical covariants suited to expansion of the NN amplitude on the full Dirac space of two nucleons, with proper regard for parity invariance, time-reversal invariance, charge symmetry, and the generalized Pauli principle. The covariants selected must be linearly independent and the associated amplitudes must be free of kinematical singularities.[10] Second, one must determine the Lorentz invariant amplitudes which multiply the kinematical covariants. In Ref. 15, a complete representation is developed which naturally embeds the IA1 assumption plus new terms which act to control to + to − couplings. All desired symmetries are incorporated. However, the Lorentz invariant amplitudes of Ref. 15 do not have simple symmetry with respect to $\vartheta \to \pi - \vartheta$. The Pauli principle is obeyed, but in a way which requires complicated combinations of amplitudes to be even or odd when $\vartheta \to \pi - \vartheta$. This occurs because some of the kinematical covariants of Ref. 15 do not transform into themselves when particle exchange operators are applied. A more symmetrical representation is developed in Ref. 16, where symmetrized covariants are developed which are even or odd with respect to particle exchange. Since the covariants are symmetric, each Lorentz invariant amplitude of the representation is even or odd when $\vartheta \to \pi - \vartheta$, for on-mass-shell kinematics. In this case, all amplitudes have been calculated in terms of 44 independent amplitudes. The analysis uses a dynamical description of the NN interaction based on the meson exchange model of van Faassen and Tjon.[18-20] The meson exchange model provides a good reproduction of the NN phase shifts in the 0–1000 MeV range for both isospin 0 and isospin 1 states.

In order to treat exchange contributions to the optical potential in a reasonable fashion, it is necessary to separate the NN amplitudes into direct and exchange parts. In the symmetrical representation of Ref. 16, this separation has been effected by the device of fitting each of the 44 independent amplitudes as a sum of Yukawa terms which explicitly is symmetric or antisymmetric with respect to $t \to u$, where t and u are Lorentz invariant Mandelstam variables. In the c.m. frame for NN scattering, $t = -2p^2[1-\cos(\vartheta)]$ and $u = -2p^2[1+\cos(\vartheta)]$, where p is the c.m. momentum. Thus when $\vartheta \to \pi - \vartheta$, $t \to u$ and vice versa. Symmetry with respect to $t \to u$ is a Lorentz invariant manifestation of the $\vartheta \to \pi - \vartheta$ symmetry which holds in the c.m. frame. Economical and accurate Yukawa fits as functions of t and u are given for each independent amplitude at proton energies of 200, 500, and 800 MeV.

Related work on the representation of the NN amplitudes is given in Ref. 17. Particularly simple covariants are used in this case. However, the corresponding amplitudes do not have simple symmetry when $\vartheta \to \pi - \vartheta$ and therefore are not as well suited to separating exchange contributions from direct ones. In principle, many different representations of the NN amplitudes are possible since the choice of covariants is not unique. All such representations are equivalent, in principle, provided one expands in a complete and linearly independent set of covariants and the associated amplitudes are determined completely.

In this paper, the symmetric, Lorentz-invariant amplitudes of Ref. 16 are used to construct a generalized impulse approximation which is called IA2. The main point is to employ a complete set of NN amplitudes from a meson-exchange model in order to provide a dynamical basis for the + to − couplings of the optical potential. Taken together with the relativistic Hartree model wave functions of Horowitz and Serot, the complete set of NN amplitudes allows a parameter-free calculation of the optical potential. Thus in IA2, a dynamical model replaces the assumption of five Fermi covariants used in IA1 with the result that + to − couplings of the Dirac optical potential are given a foundation in the meson-exchange description of the nuclear force. Complete sets of NN amplitudes are obtained from the one-boson-exchange model of van Faassen and Tjon. Coupled integral equations are solved for NN, NΔ, and $\Delta\Delta$ channels using a quasipotential reduction of the Bethe-Salpeter equation. The meson exchange model utilizes vertex cutoff functions and pseudovector πN coupling.

Section II of the paper develops a general form of the impulse approximation potential, namely $\hat{U} = -\frac{1}{4}\mathrm{Tr}_2\{\hat{\mathcal{M}}\hat{\rho}\}$, where $\hat{\mathcal{M}}$ is the Feynman amplitude for NN scattering and $\hat{\rho}$ is the relativistic nuclear density matrix. Conventionally, particle 2 is considered the target nucleon and the trace is over Dirac indices of particle 2. Wave functions of Horowitz and Serot[21] are used to construct the particle 2 density matrix, $\hat{\rho}$. Section III develops the generalized impulse approximation potential, IA2, based on complete sets of NN amplitudes. The analysis is done in momentum space. A coordinate space form of the potential is developed in Sec. IV. Utilizing the Yukawa fits of NN amplitudes to separate direct and exchange terms, a local approximation is used for the ex-

change contributions to the optical potential. In Sec. V, initial numerical calculations are presented for proton scattering by ^{40}Ca at 200, 500, and 800 MeV. A summary of this work and some concluding remarks are presented in Sec. VI.

II. IMPULSE APPROXIMATION POTENTIAL

Elementary ideas of multiple scattering theory are sufficient to suggest the "$t\rho$" optical potential appropriate for use in the Dirac equation. Following Ref. 1, consider the fixed energy Dirac equation at a given energy $E=(\hat{p}^2+m^2)^{1/2}$, $\hat{p}$ being the on-shell momentum. It has the form

$$[\gamma\cdot p - m - \hat{U}(\mathbf{r})]\psi_s(\mathbf{r})=0 , \tag{2.1}$$

where $p^\mu=(E,\mathbf{p})$ and $\gamma\cdot p=\gamma_\mu p^\mu$. Scattering from initial momentum $\mathbf{p}$ and spin projection s to final momentum $\mathbf{p}'$ and spin projection s' is described by the scattering amplitude

$$f_{s's}(\mathbf{p}',\mathbf{p})=-m(2\pi)^{-1}u_{s'}^{(+)}(\mathbf{p}')\langle\mathbf{p}'\mid\hat{T}\mid\mathbf{p}\rangle u_s^{(+)}(\mathbf{p}) , \tag{2.2}$$

where the t matrix is defined by

$$\hat{T}=\hat{U}+\hat{U}(\gamma\cdot p - m + i\epsilon)^{-1}\hat{T} . \tag{2.3}$$

A caret, as in $\hat{U}$ or $\hat{T}$, is used to denote operators on the Dirac states. Plane wave Dirac spinors used here are given by

$$u_s^{(+)}(\mathbf{p})=\left[\frac{E_\mathbf{p}+m}{2m}\right]^{1/2}\begin{bmatrix}1\\ \dfrac{\sigma\cdot\mathbf{p}}{E_\mathbf{p}+m}\end{bmatrix}\chi_s , \tag{2.4}$$

$$u_s^{(-)}(\mathbf{p})=\left[\frac{E_\mathbf{p}+m}{2m}\right]^{1/2}\begin{bmatrix}\dfrac{\sigma\cdot\mathbf{p}}{E_\mathbf{p}+m}\\ 1\end{bmatrix}\chi_s , \tag{2.5}$$

where the superscript $(+)$ or $(-)$ is used to denote positive- or negative-energy solutions of the Dirac equation.

Note that the optical theorem fixes the imaginary part of the forward scattering amplitude in terms of the total cross section σ_T and the real-to-imaginary ratio α. In the p-nucleus c.m. frame, this constraint may be written as

$$f_{ss}(\mathbf{p},\mathbf{p})/(2ip)=\sigma_T(1-i\alpha)/(8\pi) , \tag{2.6}$$

and it follows that f_{ss}/p is Lorentz invariant since σ_T and α are physical observables.

Although iterations of the potential in Eq. (2.3) are essential to a correct description, it is sufficient to consider the Born approximation, $f_{s's}^{(1)}$, in order to deduce the potential $\hat{U}$,

$$f_{s's}^{(1)}(\mathbf{p}',\mathbf{p})=-m(2\pi)^{-1}\bar{u}_{s'}^{(+)}(\mathbf{p}')\hat{U}(\mathbf{p}',\mathbf{p})u_s^{(+)}(\mathbf{p}) . \tag{2.7}$$

In the impulse approximation, the lowest order scattering amplitude is due to coherent scattering by individual nucleons of the target nucleus, regarded as free but distributed in space according to the nuclear density. For example, if the nuclear wave function is an antisymmetric product of single particle Dirac wave functions, the impulse approximation may be stated as

$$f_{s's}^{(1)}(\mathbf{p}',\mathbf{p})/(2ip)=\int\frac{d^3k}{(2\pi)^3}\sum_\alpha\bar{u}_{s'}^{(+)}(\mathbf{p}')\bar{\psi}_\alpha(\mathbf{k}+\tfrac{1}{2}\mathbf{q})\times\hat{F}(p,k-\tfrac{1}{2}q\to p',k+\tfrac{1}{2}q)\times\psi_\alpha(\mathbf{k}-\tfrac{1}{2}\mathbf{q})u_s^{(+)}(\mathbf{p}) , \tag{2.8}$$

where $\hat{F}$ is an invariant NN scattering amplitude, $q=p-p'$ is the momentum transfer, and $\psi_\alpha(\mathbf{k})$ is a bound state wave function for a nucleon with quantum numbers α. Figure 1 illustrates the single scattering process. The eigenenergy ϵ_α includes the nucleon rest energy, i.e., $\epsilon_\alpha\approx(m^2+\mathbf{k}^2)^{1/2}$. Conservation of 4-momentum requires $q^0=0$ and $k^0=\epsilon_\alpha$ in the NN amplitude and thus $p^0=p'^0=E$, where E is the proton energy. All occupied states are included in the sum over α. The factor $(2ip)^{-1}$ is needed to be consistent with our normalization convention for the invariant amplitude F, as discussed in Ref. 1. This is the same factor seen in (2.6) which relates the forward scattering amplitude to Lorentz invariant quantities.

Equality of (2.7) and (2.8) implies that the optical potential is

$$\hat{U}(\mathbf{p}',\mathbf{p})=\kappa\int\frac{d^3k}{(2\pi)^3}\bar{\psi}_\alpha(\mathbf{k}+\tfrac{1}{2}\mathbf{q})\hat{F}(p,k-\tfrac{1}{2}q\to p',k+\tfrac{1}{2}q)\times\psi_\alpha(\mathbf{k}-\tfrac{1}{2}\mathbf{q}) , \tag{2.9}$$

where

$$\kappa=\frac{-4\pi ip}{m} . \tag{2.10}$$

Positive energy spinors present in (2.8) are stripped away to obtain the potential in the Dirac space. Therefore off-shell and negative-energy matrix elements arise when $\hat{U}$ is iterated to obtain a solution to (2.3). Moreover, the bound state wave functions in (2.8) are not free Dirac spinors. Consequently, it is necessary to have the NN scattering amplitude as an operator in the full Dirac space of two nucleons in order to ensure that $\hat{U}$ is well defined. One needs the Feynman four-point function, $\hat{\mathcal{M}}$, for NN scattering in the language of quantum field theory. Indeed, the kinematic factor κ in the optical potential relates the invariant NN amplitude to a Feynman amplitude, $\hat{\mathcal{M}}$, as follows:

$$\hat{\mathcal{M}}(p,k-\tfrac{1}{2}q\to p',k+\tfrac{1}{2}q)=-\kappa\hat{F}(p,k-\tfrac{1}{2}q\to p',k+\tfrac{1}{2}q) , \tag{2.11}$$

where $\hat{\mathcal{M}}$ has the Dirac matrix elements corresponding to

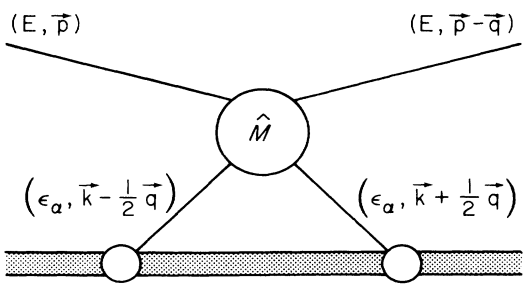

FIG. 1. Diagram for first order optical potential.

the Feynman rules of Bjorken and Drell, Ref. 22, Appendix B, as follows:

$$\overline{u_1}(\mathbf{p}_1')\overline{u_2}(\mathbf{p}_2')\hat{\mathcal{M}}(p_1p_2\to p_1'p_2')u_1(\mathbf{p}_1)u_1(\mathbf{p}_2) = i\mathcal{M}(\text{Bjorken-Drell}) . \quad (2.12)$$

Here, $\mathcal{M}$(Bjorken-Drell) refers to the sum of Feynman graphs for scattering of two nucleons from initial momenta p_1 and p_2 to final momenta p_1' and p_2'. Note that an extra factor $i=\sqrt{-1}$ is included and Dirac spinors for initial and final states are omitted to obtain $\hat{M}$ from the Feynman rules in our convention. A specific example is the sum of direct one-boson-exchange (OBE) contributions due to exchange of a scalar meson, ϵ, a neutral vector meson, ω, and a pseudoscalar meson, π, with pseudovector coupling,

$$\hat{\mathcal{M}}_{\text{OBE}}=\frac{-g_\epsilon^2}{q^2-m_\epsilon^2}+\frac{g_\omega^2\gamma_1\cdot\gamma_2}{q^2-m_\omega^2} + \frac{g_\pi^2\tau_1\cdot\tau_2}{q^2-m_\pi^2}\frac{\gamma_1^5\gamma_1\cdot(p_1-p_1')\gamma_2^5\gamma_2\cdot(p_2-p_2')}{4m^2} . \quad (2.13)$$

A second ingredient needed to construct the optical potential is the nuclear density. It is convenient to define a relativistic density matrix in the Dirac space of particle 2 as follows,

$$\hat{\rho}(\mathbf{k},\mathbf{q})=4\sum_\alpha \psi_\alpha(\mathbf{k}-\tfrac{1}{2}\mathbf{q})\overline{\psi_\alpha}(\mathbf{k}+\tfrac{1}{2}\mathbf{q}) . \quad (2.14)$$

Note that the order of the wave functions is such that $\hat{\rho}(\mathbf{k},\mathbf{q})$ is a 4×4 matrix. With these definitions, the optical potential can be written as a trace with respect to the Dirac indices of particle 2, i.e.,

$$\hat{U}(\mathbf{p}',\mathbf{p})=-\tfrac{1}{4}\text{Tr}_2\left\{\int\frac{d^3k}{(2\pi)^3}\hat{\mathcal{M}}(p,\,k-\tfrac{1}{2}q\to p',\,k+\tfrac{1}{2}q)\hat{\rho}(\mathbf{k},\mathbf{q})\right\} . \quad (2.15)$$

Thus the impulse approximation optical potential is determined by the Feynman amplitude for NN scattering and the relativistic nuclear density matrix. The analogous nonrelativistic expression[23] is very similar, i.e.,

$$\hat{U}_{\text{NR}}(\mathbf{p}',\mathbf{p})=\tfrac{1}{2}\text{Tr}_2\left\{\int\frac{d^3k}{(2\pi)^3}t(\mathbf{p},\,\mathbf{k}-\tfrac{1}{2}\mathbf{q}\to\mathbf{p}',\,\mathbf{k}+\tfrac{1}{2}\mathbf{q})\rho(\mathbf{k},\mathbf{q})\right\} , \quad (2.16)$$

where the trace is with respect to Pauli spin indices of particle 2, t is the spin-dependent t matrix, and ρ is a 2×2 density matrix for the nuclear ground state in the Pauli space. Simple arguments yield the $-\frac{1}{4}\text{Tr}_2\{\hat{\mathcal{M}}\hat{\rho}\}$ form of the optical potential in the Dirac equation. The result may be generalized by using the exact nuclear density in (2.15).

Isospin quantum numbers have been suppressed in the analysis leading to the optical potential. A straightforward extension of the analysis accounts for differing proton and neutron densities and interactions as follows:

$$\hat{U}(\mathbf{p}',\mathbf{p})=-\tfrac{1}{4}\text{Tr}_2\left\{\int\frac{d^3k}{(2\pi)^3}\hat{\mathcal{M}}_{\text{pp}}(p,\,k-\tfrac{1}{2}q\to p',\,k+\tfrac{1}{2}q)\hat{\rho}_{\text{p}}(\mathbf{k},\mathbf{q})\right\}-\tfrac{1}{4}\text{Tr}_2\left\{\int\frac{d^3k}{(2\pi)^3}\hat{\mathcal{M}}_{\text{pn}}(p,\,k-\tfrac{1}{2}q\to p',\,k+\tfrac{1}{2}q)\hat{\rho}_{\text{n}}(\mathbf{k},\mathbf{q})\right\} . \quad (2.17)$$

where $\hat{\rho}_{\text{p}}$ and $\hat{\rho}_{\text{n}}$ are proton and neutron density matrices in the nuclear ground state and $\hat{\mathcal{M}}_{\text{pp}}$ and $\hat{\mathcal{M}}_{\text{pn}}$ are Feynman amplitudes for proton-proton scattering and proton-neutron scattering, respectively.

Integration over $\mathbf{k}$ in (2.15) or (2.16) is generally approximated by evaluating the NN amplitude at $\mathbf{k}=0$ and removing it from the integral. This "factorization approximation" is motivated by the observation that the nuclear density generally varies more rapidly with $\mathbf{k}$ than the NN amplitude and is largest at $\mathbf{k}=0$. In the nonrelativistic case, $\mathbf{k}=0$ is an optimal factorization point in the sense that the leading correction proportional to $\mathbf{k}$ vanishes for a closed shell nucleus.[24] Factorization in the relativistic case yields

$$\hat{U}(\mathbf{p}',\mathbf{p})=-\tfrac{1}{4}\text{Tr}_2\{\hat{\mathcal{M}}(p,\,-\tfrac{1}{2}q\to p',\,+\tfrac{1}{2}q)\hat{\rho}(\mathbf{q})\} , \quad (2.18)$$

where $\hat{\rho}(\mathbf{q})$ is a 4×4 matrix obtained by integrating over $\mathbf{k}$,

$$\hat{\rho}(\mathbf{q})=4\int\frac{d^3k}{(2\pi)^3}\sum_\alpha\psi_\alpha(\mathbf{k}-\tfrac{1}{2}\mathbf{q})\overline{\psi_\alpha}(\mathbf{k}+\tfrac{1}{2}\mathbf{q}) . \quad (2.19)$$

Employing the Fourier transformation,

$$\psi_\alpha(\mathbf{k})=\int\frac{d^3r}{(2\pi)^3}e^{-i\mathbf{k}\cdot\mathbf{r}}\psi_\alpha(\mathbf{r}) , \quad (2.20)$$

it is straightforward to express $\hat{\rho}(\mathbf{q})$ in terms of a coordinate space density matrix

$$\hat{\rho}(\mathbf{q})=\int d^3r\,e^{i\mathbf{q}\cdot\mathbf{r}}\hat{\rho}(\mathbf{r}) , \quad (2.21)$$

$$\hat{\rho}(\mathbf{r})=4\sum_\alpha\psi_\alpha(\mathbf{r})\overline{\psi_\alpha}(\mathbf{r}) . \quad (2.22)$$

Equations (2.18)–(2.22) are the important results of this section. They define the optical potential in the factorized form used in the rest of the paper. To construct the potential, one needs the Feynman amplitude $\hat{\mathcal{M}}$ for NN scattering in the Breit frame and the nuclear density matrix $\hat{\rho}$.

In Appendix A, the relativistic density matrix is considered in detail based on relativistic Hartree wave functions for a closed shell nucleus.[21] In this case, one obtains scalar, vector, and tensor form factors as follows:

$$\hat{\rho}(\mathbf{q})=\rho_S(q)+\gamma_2^0\rho_V(q)-\frac{\boldsymbol{\alpha}_2\cdot\mathbf{q}}{2m}\rho_T(q)\ , \tag{2.23}$$

where each term is a Fourier transformation of a coordinate-space density:

$$\rho_S(q)=4\pi\int_0^\infty dr\, r^2 j_0(qr)\rho_S(r)\ , \tag{2.24}$$

$$\rho_V(q)=4\pi\int_0^\infty dr\, r^2 j_0(qr)\rho_V(r)\ , \tag{2.25}$$

$$\rho_T(q)=-4\pi m\int_0^\infty dr\, r^2\frac{j_1(qr)}{q}\rho_T(r)\ , \tag{2.26}$$

and j_m is a spherical Bessel function. Coordinate-space scalar, vector, and tensor densities are obtained from radial Dirac-Hartree wave functions with upper components $G_{nljt}(r)$ and lower components $-i\sigma_r F_{nljt}(r)$,

$$\rho_S(r)=\sum_{nljt}\frac{2j+1}{4\pi}[G^2_{nljt}(r)-F^2_{nljt}(r)]\ , \tag{2.27}$$

$$\rho_V(r)=\sum_{nljt}\frac{2j+1}{4\pi}[G^2_{nljt}(r)+F^2_{nljt}(r)]\ , \tag{2.28}$$

$$\rho_T(r)=\sum_{nljt}\frac{2j+1}{4\pi}[4G_{nljt}(r)+F_{nljt}(r)]\ . \tag{2.29}$$

Here, n is the radial quantum number, l and j are angular momentum quantum numbers, and $t=+\frac{1}{2}$ for proton states and $t=-\frac{1}{2}$ for neutron states. To obtain the proton or neutron densities, $\hat{\rho}_p$ and $\hat{\rho}_n$, for use in (2.17), one uses (2.23) with scalar, vector, and tensor terms obtained by omitting the sum over t in (2.27)–(2.29).

Figure 2 shows the nuclear form factors for ^{40}Ca based on Eqs. (2.24)–(2.26) and using the Hartree wave functions of Horowitz and Serot.[21] The tensor form factor defined as in (2.26) is as large as the scalar or vector form factors; however, it should be noted that the factor $\mathbf{q}/(2m)$ tends to suppress tensor contributions to the optical potential. Since $\rho_V(q)$ is the matter form factor, in practice it is the same as the nonrelativistic form factor, $\rho_{NR}(q)$. Relativistic effects in the nuclear density show up as differences between $\rho_V(q)$ and either $\rho_S(q)$ or $\rho_T(q)$. To see that this is the case, consider single-particle wave functions formed by attaching free Dirac spinors to nonrelativistic wave functions ϕ_α, i.e.,

$$\psi_\alpha(\mathbf{k})\approx\begin{bmatrix}1\\ \dfrac{\boldsymbol{\sigma}\cdot\mathbf{k}}{2m}\end{bmatrix}\phi_\alpha(\mathbf{k})\ , \tag{2.30}$$

where terms of order $\mathbf{k}^2/m^2$ are neglected. From (2.19) one finds that the corresponding density is

$$\hat{\rho}(\mathbf{q})=\left[1+\gamma_2^0-\frac{\boldsymbol{\alpha}_2\cdot\mathbf{q}}{2m}\right]\rho_{NR}(q)\ , \tag{2.31}$$

where $\rho_{NR}(q)$ is the nonrelativistic form factor. Terms of order $\mathbf{k}^2/m^2$ are again neglected. Thus it is clear that $\rho_S=\rho_V=\rho_T=\rho_{NR}$ when wave functions of the form (2.30) are used.

III. CONSTRUCTION OF THE POTENTIAL

In general, the parity-invariant NN amplitude needed to construct the Dirac optical potential contains 128 terms for each isospin. However, not all 128 terms are independent. Charge symmetry and time-reversal invariance reduce the number of independent amplitudes to 56 for off-mass-shell kinematics, to 50 for quasipotential kinematics, and to 44 for on-mass-shell kinematics, again for each isospin.[15,16] Moreover, the on-mass-shell case can be characterized by invariant amplitudes which are individually even or odd with respect to the generalized Pauli principle. Only five of the 44 independent amplitudes needed on mass shell are determined directly from phase shift analysis of NN scattering data and therefore the others must be predicted from a theoretical model. For this purpose, the only viable option is a meson exchange model. Extensive analysis of NN scattering dynamics within the meson exchange framework has been carried out in recent years. Of particular relevance is the work of Refs. 18 and 19 in which the NN scattering analysis is done in a relativistic framework. Recently, the model has been extended to incorporate channel couplings between NN, NΔ, and ΔΔ states in order to allow for inelasticity in the NN channel and to obtain realistic results above the pion production threshold. Numerical calculations show that a reasonably accurate description of NN scattering data is achieved for the 0–1000 MeV range of laboratory energy. Within this dynamical framework, one has a complete description of the relativistic NN amplitude. Therefore we adopt the meson exchange model as the theoretical input to determine negative energy couplings implied by the Dirac optical potential.

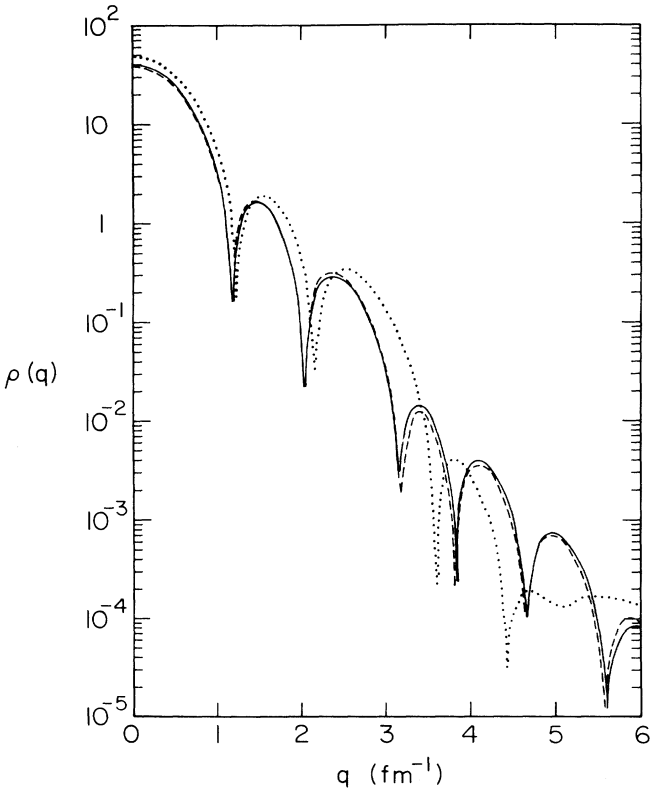

FIG. 2. Nuclear form factors for ^{40}Ca. Solid line shows vector form factor, dashed line shows scalar form factor, and dotted line shows tensor form factor.

A relativistic quasipotential equation is solved for coupled NN, NΔ, and ΔΔ states with π, ϵ, η, ρ, δ, and ω meson exchange. The meson exchange dynamics predicts the NN matrix elements involving negative energy states from the same meson-baryon couplings which succeed to describe the NN scattering in positive energy states. Pseudovector πN coupling is used. Since phenomenological phase shifts are available in positive energy states, these are used in place of the meson exchange results to ensure accuracy. References 18 and 19 describe the meson exchange model and further details may be found in the thesis of van Faassen.[20] In our calculations, the model is extended to include negative-energy intermediate states in the NN channel.[15]

For the optical potential, NN amplitudes are needed in the proton-nucleus c.m. frame. Phase shift analysis is practical for NN scattering only in the NN c.m. frame. Therefore it is necessary to boost the amplitudes. This is most conveniently done by introducing a Lorentz invariant representation in which amplitudes take the same form in all frames. References 15–17 address the problem of expanding the full amplitude in terms of invariant amplitudes times kinematic covariants. In particular, Ref. 16 provides a highly symmetrical set of kinematic covariants for which all independent amplitudes are even or odd with respect to the generalized Pauli principle for on-mass-shell kinematics. Moreover, Yukawa fits are given for each of the independent amplitudes and symmetry relations permit reconstruction of a complete set of 128 amplitudes from the independent amplitudes. Symmetry with respect to Pauli exchange is incorporated by appropriately combining Yukawa functions of t and u, the Mandelstam invariants. The Yukawa fits are designed to provide a separation of direct and exchange contributions for on-mass-shell scattering and they provide an analytical form suitable for extrapolating amplitudes beyond the physical region.

Following Ref. 16, the full NN amplitude is expanded in two steps. Step 1 uses covariant projection operators to separate positive and negative-energy sectors of the Dirac space,

$$\hat{F}(p_1,p_2\to p_1',p_2') = \sum_{\rho_1'\rho_2'\rho_1\rho_2} \Lambda_1^{\rho_1'}(\mathbf{p}_1')\Lambda_2^{\rho_2'}(\mathbf{p}_2') \times \hat{F}^{ij}(p_1,p_2\to p_1',p_2') \times \Lambda_1^{\rho_1}(\mathbf{p}_1)\Lambda_2^{\rho_2}(\mathbf{p}_2) , \quad (3.1)$$

where $\rho_i = +$ or $-$, for $i=1$ and 2, distinguishes positive and negative energy initial states. Similarly, $\rho_i' = +$ or $-$ for final states. There are 16 ρ-spin sectors of the scattering matrix of two nucleons and a class superscript ij is associated to each as in Table I. Covariant projection operators which are used to separate the 16 sectors of the full Dirac space are defined as follows,

$$\Lambda^{\rho}(\mathbf{p}) = \frac{\rho(E_{\mathbf{p}} - \boldsymbol{\gamma}\cdot\mathbf{p}) + m}{2m} , \quad (3.2)$$

Where $\rho = +$ or $-$. Note that amplitudes $\hat{F}^{ij}$ are restricted to act only within one ρ-spin sector. Thus there are 16 different sets of $\hat{F}^{ij}$ amplitudes which go into determining the operator $\hat{F}$ defined by (3.1).

TABLE I. The 16 ρ-spin sectors of the scattering matrix of two nucleons.

Class	Rho spins			
ij	$\rho_1'\rho_1$	$\rho_2'\rho_2$	η_{ij}	Constraint
11	+ +	+ +	+	$f_6^{11}=0$
12	+ +	− +	+	$f_6^{12}=0$
21	− +	+ +	+	$f_6^{21}=0$
13	+ +	+ −	−	$f_6^{13}=0$
31	+ −	+ +	−	$f_6^{31}=0$
14	+ +	− −	+	$f_9^{14}=0$
41	− −	+ +	+	$f_9^{41}=0$
23	− +	+ −	−	$f_9^{23}=0$
32	+ −	− +	−	$f_9^{32}=0$
22	− +	− +	+	$f_8^{22}=0$
33	+ −	+ −	−	$f_8^{33}=0$
24	− +	− −	+	$f_6^{24}=0$
42	− −	− +	+	$f_6^{42}=0$
34	+ −	− −	−	$f_6^{34}=0$
43	− −	+ −	−	$f_6^{43}=0$
44	− −	− −	+	$f_6^{44}=0$

Step 2 expands each $\hat{F}^{ij}$ in terms of invariant amplitudes f_k^{ij} times kinematic covariants $\Gamma_k(+)$ or $\Gamma_k(-)$ as follows,

$$\hat{F}^{ij}(p_1,p_2\to p_1',p_2') = \sum_{k=1}^{9} f_k^{ij}[a_1]\Gamma_k(\eta_{ij}) , \quad (3.3)$$

with $\eta_{ij} = +$ or $-$ depending on the class ij. Table I provides values of η_{ij} which are used in the various ρ-spin sectors. The notation $[a_1]$ refers to the set of Lorentz invariant arguments upon which each amplitude depends. These arguments are defined in Table III of Ref. 16. However, for on-mass-shell kinematics, just three arguments are needed, i.e., $s=(p_1+p_2)^2$, $t=(p_1-p_2)^2$, and $u=(p_1-p_2')^2$. As explained in Ref. 16, the covariants $\Gamma_k(\eta)$ are even or odd with respect to particle exchange. Although nine terms appear in Eq. (3.3), one of these is identically zero for each of the 16 classes due to a constraint shown in Table I. Thus Eq. (3.1) with 16 independent ρ-spin sectors and Eq. (3.3) with eight independent amplitudes for each sector accounts for 128 linearly independent terms and 128 invariant amplitudes. Due to symmetries, only 44 of the invariant amplitudes are independent on mass shell. Moreover, one of these is found to vanish when a quasipotential calculation of the NN amplitudes is performed. Thus 43 independent amplitudes suffice to describe all nonvanishing f_n^{ij} on mass shell.

Using the Yukawa fits to the independent amplitudes from Ref. 16, we construct a complete set of on-mass-shell amplitudes as follows:

$$f_n^{11} = -\kappa^{-1}[\mathcal{M}_n^{11}(t) + \sigma_n^{11}\mathcal{M}_n^{11}(u)], \quad n=1-5 \quad (3.4)$$

$$f_n^{12}=f_n^{21}=f_n^{13}=f_n^{31}=-\kappa^{-1}[\mathcal{M}_n^{12}(t)+\sigma_n^{12}\mathcal{M}_n^{12}(u)]\ , \quad n=1\text{–}5,\ 7\text{–}9 \tag{3.5}$$

$$f_n^{22}=f_n^{33}=-\kappa^{-1}[\mathcal{M}_n^{22}(t)+\sigma_n^{22}\mathcal{M}_n^{22}(u)],\quad n=1\text{–}6 \tag{3.6}$$

$$f_n^{24}=f_n^{42}=f_n^{34}=f_n^{43}=-\kappa^{-1}[\mathcal{M}_n^{24}(t)+\sigma_n^{24}\mathcal{M}_n^{24}(u)]\ , \quad n=1\text{–}5,\ 7\text{–}9 \tag{3.7}$$

$$f_n^{44}=-\kappa^{-1}[\mathcal{M}_n^{44}(t)+\sigma_n^{44}\mathcal{M}_n^{44}(u)],\quad n=1\text{–}5 \tag{3.8}$$

$$g_n^{+}=-\kappa^{-1}[\mathcal{M}_n^{14}(t)+\sigma_n^{14}\mathcal{M}_n^{14}(u)],\quad n=1\text{–}6 \tag{3.9}$$

$$g_n^{-}=-\kappa^{-1}[\mathcal{M}_n^{23}(t)+\sigma_n^{23}\mathcal{M}_n^{23}(u)],\quad n=1\text{–}5 \tag{3.10}$$

$$f_n^{14}=f_n^{41}=\tfrac{1}{2}(g_n^{+}+g_n^{-}),\quad n=1,6 \tag{3.11}$$

$$f_n^{23}=f_n^{32}=\tfrac{1}{2}(g_n^{+}-g_n^{-}),\quad n=1,6 \tag{3.12}$$

where $\mathcal{M}_n^{ij}(t)$ represents a sum of four Yukawa terms as follows:

$$\mathcal{M}_n^{ij}(t)=\sum_{m=1}^{4}\frac{(g_{nm}^{ij})^2}{\mu_m^2-t}\frac{\Lambda^2}{\Lambda^2-t}\ , \tag{3.13}$$

and, similarly, $\mathcal{M}_n^{ij}(u)$ is the same function with $t\to u$. Symmetry parameters σ_n^{ij} take the values $+1$ or -1 and thus each amplitude in Eqs. (3.4)–(3.10) is symmetric or antisymmetric with respect to interchange of t and u. Numerical values of coupling constants $(g_{nm}^{ij})^2/(4\pi)$, symmetry parameters σ_n^{ij}, masses μ_m, and cutoff mass Λ, which are needed to evaluate (3.13) for the 43 independent amplitudes of Eqs. (3.4)–(3.10), are tabulated in Ref. 16 for both isospin 0 and isospin 1 states. A cutoff mass $\Lambda=1150$ MeV is used.

The f_n^{11} amplitudes are based on a phase shift analysis of NN scattering data as given in Ref. 25. As a result, the f_n^{11} amplitudes for isospin 0 states are not symmetric with respect to interchange of t and u and a correction must be made. Charge dependence of the np interaction is incorporated into the phase shift analysis and this causes the small asymmetry with respect to interchange of t and u. To take this effect into account, we add to f_n^{11} (in isospin 0 states) a correction δf_n^{11} which has opposite symmetry to that of f_n^{11}, i.e.,

$$\delta f_n^{11}=-\kappa^{-1}[\delta\mathcal{M}_n^{11}(t)-\sigma_n^{11}\delta\mathcal{M}_n^{11}(u)],\quad n=1\text{–}5 \tag{3.14}$$

$$\delta\mathcal{M}_n^{11}(t)=\sum_{m=1}^{4}\frac{(\delta g_{nm}^{11})^2}{\mu_m^2-t}\frac{\Lambda^2}{\Lambda^2-t}\ . \tag{3.15}$$

The five extra coupling constants $(\delta g_{nm}^{11})^2/(4\pi)$ in (3.15) are the charge-dependent coupling constants listed in Ref. 16 for isospin 0 states.

Equations (3.4)–(3.15) completely determine 110 nonvanishing terms of the on-mass-shell NN interaction on the full Dirac space of two nucleons. Time reversal invariance, charge symmetry, and the generalized Pauli Principle produce equalities among the amplitudes which are evident in these equations.

For the present purpose, it is convenient to expand the symmetrized covariants $\Gamma_k(\eta)$ of (3.3) in terms of 13 simpler ones as follows,

$$\Gamma_k(\eta)=\sum_{n=1}^{13}B_{kn}(\eta)\mathcal{K}_n\ . \tag{3.16}$$

Table II defines covariants $\mathcal{K}_1$ to $\mathcal{K}_{13}$ in terms of Dirac matrices and momenta Q_{11}, Q_{12}, Q_{21}, and Q_{22} which are formed out of the initial momenta p_1 and p_2 and final momenta p_1' and p_2' as follows,

$$Q_{ij}=(p_i'+p_j)/(2m)\ . \tag{3.17}$$

Table II also provides values for the 9×13 matrix $B(\eta)$. Equation (3.16) and Table II constitute a representation of the symmetrized covariants $\Gamma_k(\eta)$.

It follows that $\Gamma_k(\eta)$ may be replaced by linear combinations of $\mathcal{K}_1$ to $\mathcal{K}_{13}$ to arrive at

$$\hat{F}^{ij}(p_1,p_2\to p_1',p_2')=\sum_{n=1}^{13}F_n^{ij}[a_1]\mathcal{K}_n\ , \tag{3.18}$$

where

$$F_n^{ij}[a_1]=\sum_{k=1}^{9}f_k^{ij}[a_1]B_{kn}(\eta_{ij})\ . \tag{3.19}$$

Covariants $\mathcal{K}_1$ to $\mathcal{K}_9$ and the associated amplitudes F_1^{ij} to F_9^{ij} were used in Ref. 15 to construct a nine-term representation in which F_{10} to F_{13} are zero. The nine-term representation incorporates all the required symmetries, but it produces amplitudes which do not, in general, have simple symmetry with respect to interchange of t and u. This feature complicates the separation of direct and exchange contributions and therefore limits the usefulness of the Ref. 15 representation to high energy where exchange contributions to the optical potential are suppressed. It should be clear that Eq. (3.18) applies to either the nine term representation of Ref. 15 or to the symmetrized representation of Ref. 16. In the latter case, Eq. (3.19) and Table II show how to construct the 13 amplitudes F_n^{ij} from the nine symmetrized amplitudes f_n^{ij} given by Eqs. (3.4)–(3.12).

To determine the optical potential, we need the Feynman amplitude $\hat{\mathcal{M}}$. From Eqs. (2.11), (3.1), and (3.18), it follows that

$$\hat{\mathcal{M}}(p_1,p_2\to p_1',p_2')=\sum_{\rho_1'\rho_2'\rho_1\rho_2}\Lambda_1^{\rho_1'}(\mathbf{p}_1')\Lambda_2^{\rho_2'}(\mathbf{p}_2')\left[\sum_{n=1}^{13}M_n^{\rho_1'\rho_2'\rho_1\rho_2}[a_1]\mathcal{K}_n\right]\Lambda_1^{\rho_1}(\mathbf{p}_1)\Lambda_2^{\rho_2}(\mathbf{p}_2)\ , \tag{3.20}$$

where $\mathcal{M}_n^{\rho_1'\rho_2'\rho_1\rho_2}[a_1]$ is a scalar Feynman amplitude formed as follows,

$$\mathcal{M}_n^{\rho_1'\rho_2'\rho_1\rho_2}[a_1]=-\kappa F_n^{ij}[a_1]\ . \tag{3.21}$$

Table I specifies the correspondence of ρ-spin labels, $\rho_1'\rho_2'\rho_1\rho_2$, which appear on the left-hand side of this equation, to class labels ij, which appear on the right-hand side.

Substituting (3.20) into (2.18) yields, after some rearrangement,

TABLE II. Matrix $B(\eta)$. Row defines the covariants $\mathcal{K}_1$ to $\mathcal{K}_{13}$ in terms of Dirac matrices and momenta Q_{11}, Q_{12}, Q_{21}, and Q_{22} defined as in Eq. (3.4). $\tilde{S}$ is the Fierz exchange operator. Rows 3–11 define the symmetrized covariants Γ_1 to Γ_9 in terms of simpler covariants $\mathcal{K}_1$ to $\mathcal{K}_{13}$ by providing values for the 9×13 matrix $B(\eta)$ in Eq. (3.3). The parameter η may be $+1$ or -1 depending on the class.

$\mathcal{K}_n$ \	$\mathcal{K}_1$	$\mathcal{K}_2$	$\mathcal{K}_3$	$\mathcal{K}_4$	$\mathcal{K}_5$	$\mathcal{K}_6$	$\mathcal{K}_7$	$\mathcal{K}_8$	$\mathcal{K}_9$	$\mathcal{K}_{10}$	$\mathcal{K}_{11}$	$\mathcal{K}_{12}$	$\mathcal{K}_{13}$
	1	$\gamma_1\cdot\gamma_2$	$\sigma_1^{\mu\nu}\sigma_{2\mu\nu}$	$\gamma_1^5\gamma_2^5$	$\gamma_1^5\gamma_1^\mu\gamma_2^5\gamma_{2\mu}$	$\gamma_2\cdot Q_{11}$	$\gamma_1\cdot Q_{22}$	$P\gamma_2\cdot Q_{11}$	$P\gamma_1\cdot Q_{22}$	$\gamma_2\cdot Q_{12}\tilde{S}$	$\gamma_1\cdot Q_{21}\tilde{S}$	$P\gamma_2\cdot Q_{12}\tilde{S}$	$P\gamma_1\cdot Q_{21}\tilde{S}$
Γ_1	$\frac{3}{4}$	$-\frac{1}{4}$	$-\frac{1}{8}$	$-\frac{1}{4}$	$\frac{1}{4}$	0	0	0	0	0	0	0	0
Γ_2	$\frac{3}{2}$	0	$\frac{1}{4}$	$\frac{3}{2}$	0	0	0	0	0	0	0	0	0
Γ_3	-1	$-\frac{1}{2}$	0	1	$-\frac{3}{2}$	0	0	0	0	0	0	0	0
Γ_4	1	$\frac{1}{2}$	0	-1	$-\frac{1}{2}$	0	0	0	0	0	0	0	0
Γ_5	$-\frac{1}{4}$	$\frac{1}{4}$	$-\frac{1}{8}$	$\frac{3}{4}$	$-\frac{1}{4}$	0	0	0	0	0	0	0	0
Γ_6	0	0	0	0	0	1	1	0	0	1	1	0	0
$\Gamma_7(\eta)$	0	0	0	0	0	1	-1	0	0	$-\eta$	η	0	0
$\Gamma_8(\eta)$	0	0	0	0	0	0	0	η	η	0	0	η	η
$\Gamma_9(\eta)$	0	0	0	0	0	0	0	η	$-\eta$	0	0	1	-1

$$\hat{U}(\mathbf{p}',\mathbf{p})=\sum_{\rho_1'\rho_1}\Lambda_1^{\rho_1'}(\mathbf{p}')\hat{U}^{\rho_1'\rho_1}(\mathbf{p}',\mathbf{p})\Lambda_1^{\rho_1}(\mathbf{p})\ , \tag{3.22}$$

where

$$\hat{U}^{\rho_1'\rho_1}(\mathbf{p}',\mathbf{p})=-\sum_{\rho_2'\rho_2}\sum_{n=1}^{13}\mathcal{M}_n^{\rho_1'\rho_2'\rho_1\rho_2}[a_1]\tfrac{1}{4}\mathrm{Tr}_2\{\mathcal{K}_n\hat{\rho}^{\rho_2\rho_2'}(\mathbf{q})\} \tag{3.23}$$

and

$$\hat{\rho}^{\rho_2\rho_2'}(\mathbf{q})=\Lambda_2^{\rho_2}(-\tfrac{1}{2}\mathbf{q})\hat{\rho}(\mathbf{q})\Lambda_2^{\rho_2'}(\tfrac{1}{2}\mathbf{q})\ . \tag{3.24}$$

Invariance of a trace with respect to cyclic permutations has been used to move $\Lambda_2^{\rho_2'}(\frac{1}{2}\mathbf{q})$ to a rightmost position, and then absorb it into the projected density operator defined by (3.24). Equation (3.23) defines four optical potentials, $\hat{U}^{++}$, $\hat{U}^{+-}$, $\hat{U}^{-+}$, and $\hat{U}^{--}$, as sums of direct and exchange Feynman amplitudes times traces involving density operators ρ^{++}, ρ^{+-}, ρ^{-+}, and ρ^{--} and kinematical covariants $\mathcal{K}_1$ to $\mathcal{K}_{13}$.

Consider first the projected densities. Using (2.23) in (3.24) leads to the following results,

$$\hat{\rho}^{\rho_2\rho_2'}(\mathbf{q})=\sum_k\rho_k^{\rho_2\rho_2'}(q)\chi_k(2)\ , \tag{3.25}$$

where $\rho_k^{\rho_2\rho_2'}(q)$ are form factors depending only on $q=|\mathbf{q}|$, and $\chi_k(2)$ denotes a set of eight linearly independent and parity invariant matrices in the Dirac space of particle 2. For example, these may be chosen to be

$$\chi_k=\{1,\gamma^0,\boldsymbol{\alpha}\cdot\hat{\mathbf{e}}_1,\boldsymbol{\gamma}\cdot\hat{\mathbf{e}}_1,\boldsymbol{\alpha}\cdot\hat{\mathbf{e}}_2,\boldsymbol{\gamma}\cdot\hat{\mathbf{e}}_2,\boldsymbol{\alpha}\cdot\hat{\mathbf{e}}_2\boldsymbol{\alpha}\cdot\hat{\mathbf{e}}_1,\gamma\cdot\hat{\mathbf{e}}_2\boldsymbol{\alpha}\cdot\hat{\mathbf{e}}_1\}\ ,$$

where $\hat{\mathbf{e}}_1$ and $\hat{\mathbf{e}}_2$ are orthogonal unit vectors. For the present purpose, it is convenient to use vectors which are natural to the optical potential, even though they are neither orthogonal nor unit vectors. Therefore, the set of χ's which we use is based on the choices $\hat{\mathbf{e}}_1\rightarrow\mathbf{q}/m$ and $\hat{\mathbf{e}}_2\rightarrow\mathbf{p}/m$, where $\mathbf{q}=\mathbf{p}-\mathbf{p}'$, and where $\mathbf{p}$ and $\mathbf{p}'$ are the momentum arguments of the optical potential. The set of χ's used is

$$\chi_k=\left\{1,\gamma^0,\frac{-\boldsymbol{\alpha}\cdot\mathbf{q}}{m},\frac{\boldsymbol{\gamma}\cdot\mathbf{q}}{m},\frac{\boldsymbol{\alpha}\cdot\mathbf{p}}{m},\frac{\boldsymbol{\gamma}\cdot\mathbf{p}}{m},\frac{\boldsymbol{\alpha}\cdot\mathbf{p}\boldsymbol{\alpha}\cdot\mathbf{q}}{m^2},\frac{\boldsymbol{\gamma}\cdot\mathbf{p}\boldsymbol{\alpha}\cdot\mathbf{q}}{m^2}\right\}. \tag{3.26}$$

For example, $\chi_3(2)=-\boldsymbol{\alpha}_2\cdot\mathbf{q}/m$ and so on, where the Dirac matrices for particle 2 are used. One similarly has a set $\chi_k(1)$ in which the Dirac matrices of particle 1 are used. Any parity invariant operator on the Dirac space of particle 2 may be expanded, as in (3.25), in the set of $\chi_k(2)$. Similarly, any parity invariant operator on the Dirac space of particle 1 may be expanded in the set $\chi_k(1)$.

An important property of the χ's is that they form a group with the multiplication rule

$$\chi_i\chi_j=\sum_k\phi_{ijk}\chi_k\ , \tag{3.27}$$

where the structure constants ϕ_{ijk} depend on the scalar

products $a=\hat{\mathbf{e}}_1\cdot\hat{\mathbf{e}}_1$, $b=\hat{\mathbf{e}}_2\cdot\hat{\mathbf{e}}_2$, and $c=\hat{\mathbf{e}}_1\cdot\hat{\mathbf{e}}_2$. If $\hat{\mathbf{e}}_1$ and $\hat{\mathbf{e}}_2$ are orthogonal, then the sum on the right-hand side of (3.27) contains a single term. Otherwise there can be two terms. Table III shows the group structure constants ϕ_{ijk} based on our choices $\hat{\mathbf{e}}_1\rightarrow\mathbf{q}/m$ and $\hat{\mathbf{e}}_2\rightarrow\mathbf{p}/m$. Note that Dirac traces of χ's vanish except for the scalar term χ_1, i.e.,

$$\tfrac{1}{4}\mathrm{Tr}\{\chi_k\}=\delta_{k1},\quad k=1-8\ . \tag{3.28}$$

For the Hartree-density of a closed-shell nucleus, only χ_1 to χ_4 have nonvanishing coefficients in (3.25). The nonvanishing form factors are

$$\rho_1^{\rho_2\rho_2'}(q)=\tfrac{1}{4}[1+\rho_2\rho_2'(\lambda^2+a^2)]\rho_S(q)+\tfrac{1}{4}\lambda(\rho_2+\rho_2')\rho_V(q) -\tfrac{1}{2}\rho_2\rho_2'\lambda a^2\rho_T(q)\ , \tag{3.29}$$

$$\rho_2^{\rho_2\rho_2'}(q)=\tfrac{1}{4}\lambda(\rho_2+\rho_2')\rho_S(q)+\tfrac{1}{4}(1+\rho_2\rho_2')\rho_V(q) -\tfrac{1}{4}(\rho_2+\rho_2')a^2\rho_T(q)\ , \tag{3.30}$$

$$\rho_3^{\rho_2\rho_2'}(q)=\tfrac{1}{4}\lambda\rho_2\rho_2'\rho_T(q)+\tfrac{1}{8}(\rho_2+\rho_2')\rho_V(q) -\tfrac{1}{8}[1-\rho_2\rho_2'(\lambda^2+a^2)]\rho_T(q)\ , \tag{3.31}$$

$$\rho_4^{\rho_2\rho_2'}(q)=\tfrac{1}{8}(\rho_2-\rho_2')[\rho_S(q)-\lambda\rho_V(q)]\ , \tag{3.32}$$

where

$$a^2=q^2/(4m^2) \tag{3.33}$$

and

$$\lambda=(1+a^2)^{1/2}\ . \tag{3.34}$$

Equations (3.29)–(3.34) together with (2.24)–(2.29) completely specify the nuclear density information needed to construct the optical potential in the approximation considered here.

It remains to evaluate the Dirac traces. Combining (3.23) and (3.25) produces

$$\hat{U}^{\rho_1'\rho_1}(\mathbf{p}',\mathbf{p})=-\sum_{\rho_2'\rho_2}\sum_{n=1}^{13}\sum_{k=1}^{4}\mathcal{M}_n^{\rho_1'\rho_2'\rho_1\rho_2}[a_1]\rho_k^{\rho_2\rho_2'}(q) \times\tfrac{1}{4}\mathrm{Tr}_2\{\mathcal{K}_n\chi_k(2)\}\ . \tag{3.35}$$

The required traces are straightforward and Appendix B provides details of their evaluation. Table IV lists the 13×4 matrix by Dirac traces which arise here. The results involve momenta Q_{11}, Q_{12}, Q_{21}, and Q_{22} defined as in (3.17). For the factorized optical potential ($\mathbf{k}=0$ in Fig. 1), these momenta are

$$Q_{11}=\left\{\frac{E(\mathbf{p}')+E(\mathbf{p})}{2m},\frac{\mathbf{p}-\frac{1}{2}\mathbf{q}}{m}\right\}, \tag{3.36}$$

$$Q_{12}=\left\{\frac{E(\mathbf{p}')+E(\tfrac{1}{2}\mathbf{q})}{2m},\frac{\mathbf{p}-\frac{3}{2}\mathbf{q}}{2m}\right\}, \tag{3.37}$$

$$Q_{21}=\left\{\frac{E(\mathbf{p})+E(\tfrac{1}{2}\mathbf{q})}{2m},\frac{\mathbf{p}+\frac{1}{2}\mathbf{q}}{2m}\right\}, \tag{3.38}$$

$$Q_{22}=\left\{\frac{E(\tfrac{1}{2}\mathbf{q})}{m},0\right\}. \tag{3.39}$$

Since a trace over particle-2 Dirac indices leaves an operator in the Dirac space of particle 1, the trace in (3.35) may

TABLE III. Traces for Eq. (3.35). Traces of the form $\frac{1}{4}\mathrm{Tr}_2\{\mathcal{K}_n\chi_k(2)\}$ are given. Column 3 refers to $\chi_1=1$, column 4 to $\chi_2=\gamma_2^0$, column 5 to $\chi_3=-\boldsymbol{\alpha}_2\cdot\mathbf{q}/m$, and column 6 to $\chi_4=\boldsymbol{\gamma}_2\cdot\mathbf{q}/m$.

n	$\mathcal{K}_n$	$\frac{1}{4}\mathrm{Tr}_2\{\mathcal{K}_n\}$	$\frac{1}{4}\mathrm{Tr}_2\{\mathcal{K}_n\gamma_2^0\}$	$\frac{1}{4}\mathrm{Tr}_2\left\{\mathcal{K}_n\frac{-\boldsymbol{\alpha}_2\cdot\mathbf{q}}{m}\right\}$	$\frac{1}{4}\mathrm{Tr}_2\left\{\mathcal{K}_n\frac{\boldsymbol{\gamma}_2\cdot\mathbf{q}}{m}\right\}$
1	1	1	0	0	0
2	$\boldsymbol{\gamma}_1\cdot\boldsymbol{\gamma}_2$	0	$\boldsymbol{\gamma}_1^0$	0	$\frac{\boldsymbol{\gamma}_1\cdot\mathbf{q}}{m}$
3	$\sigma_1^{\mu\nu}\sigma_{2\mu\nu}$	0	0	$-2\frac{\boldsymbol{\alpha}_1\cdot\mathbf{q}}{m}$	0
4	$P=\gamma_1^5\gamma_2^5$	0	0	0	0
5	$\gamma_1^5\gamma_1^\mu\gamma_2^5\gamma_{2\mu}$	0	0	0	0
6	$\boldsymbol{\gamma}_2\cdot\mathbf{Q}_{11}$	0	$\mathbf{Q}_{11}^0$	0	$\frac{\mathbf{Q}_{11}\cdot\mathbf{q}}{m}$
7	$\boldsymbol{\gamma}_1\cdot\mathbf{Q}_{22}$	$\boldsymbol{\gamma}_1\cdot\mathbf{Q}_{22}$	0	0	0
8	$P\boldsymbol{\gamma}_2\cdot\mathbf{Q}_{11}$	0	0	0	0
9	$P\boldsymbol{\gamma}_1\cdot\mathbf{Q}_{22}$	0	0	0	0
10	$\boldsymbol{\gamma}_2\cdot\mathbf{Q}_{12}\tilde{S}$	$\frac{1}{4}\boldsymbol{\gamma}_1\cdot\mathbf{Q}_{12}$	$\frac{1}{4}\boldsymbol{\gamma}_1^0\boldsymbol{\gamma}_1\cdot\mathbf{Q}_{12}$	$\frac{-\boldsymbol{\alpha}_1\cdot\mathbf{q}}{4m}\boldsymbol{\gamma}_1\cdot\mathbf{Q}_{12}$	$\frac{\boldsymbol{\gamma}_1\cdot\mathbf{q}}{4m}\boldsymbol{\gamma}_1\cdot\mathbf{Q}_{12}$
11	$\boldsymbol{\gamma}_1\cdot\mathbf{Q}_{21}\tilde{S}$	$\frac{1}{4}\boldsymbol{\gamma}_1\cdot\mathbf{Q}_{21}$	$\frac{1}{4}\boldsymbol{\gamma}_1\cdot\mathbf{Q}_{21}\boldsymbol{\gamma}_1^0$	$-\boldsymbol{\gamma}_1\cdot\mathbf{Q}_{21}\frac{\boldsymbol{\alpha}_1\cdot\mathbf{q}}{4m}$	$\boldsymbol{\gamma}_1\cdot\mathbf{Q}_{21}\frac{\boldsymbol{\gamma}_1\cdot\mathbf{q}}{4m}$
12	$P\boldsymbol{\gamma}_2\cdot\mathbf{Q}_{12}\tilde{S}$	$\frac{1}{4}\boldsymbol{\gamma}_1\cdot\mathbf{Q}_{12}$	$-\frac{1}{4}\boldsymbol{\gamma}_1^0\boldsymbol{\gamma}_1\cdot\mathbf{Q}_{12}$	$\frac{-\boldsymbol{\alpha}_1\cdot\mathbf{q}}{4m}\boldsymbol{\gamma}_1\cdot\mathbf{Q}_{12}$	$\frac{\boldsymbol{\gamma}_1\cdot\mathbf{q}}{4m}\boldsymbol{\gamma}_1\cdot\mathbf{Q}_{12}$
13	$P\boldsymbol{\gamma}_1\cdot\mathbf{Q}_{21}\tilde{S}$	$-\frac{1}{4}\boldsymbol{\gamma}_1\cdot\mathbf{Q}_{21}$	$\frac{1}{4}\boldsymbol{\gamma}_1\cdot\mathbf{Q}_{21}\boldsymbol{\gamma}_1^0$	$\boldsymbol{\gamma}_1\cdot\mathbf{Q}_{21}\frac{\boldsymbol{\alpha}_1\cdot\mathbf{q}}{4m}$	$\boldsymbol{\gamma}_1\cdot\mathbf{Q}_{21}\frac{\boldsymbol{\gamma}_1\cdot\mathbf{q}}{4m}$

TABLE IV. Group constants ϕ_{ijk}. Row i, column j entry shows $\sum_k \phi_{ijk}\chi_k$ in terms of three constants: $a=\mathbf{q}^2/m^2$, $b=\mathbf{p}^2/m^2$, and $c=2\mathbf{q}\cdot\mathbf{p}/m^2$. For example, from the row 4, column 5 entry, one reads $\phi_{452}=c$ and $\phi_{458}=-1$. All values of ϕ_{ijk} for i, j, or $k=1$ to 8 that are not determined by the table are zero.

	1	2	3	4	5	6	7	8
1	χ_1	χ_2	χ_3	χ_4	χ_5	χ_6	χ_7	χ_8
2	χ_2	χ_1	$-\chi_4$	$-\chi_3$	χ_6	χ_5	χ_8	χ_7
3	χ_3	χ_4	$a\chi_1$	$a\chi_2$	$-c\chi_1+\chi_7$	$c\chi_2-\chi_8$	$c\chi_3+a\chi_5$	$c\chi_4-a\chi_6$
4	χ_4	χ_3	$-a\chi_2$	$-a\chi_1$	$c\chi_2-\chi_8$	$-c\chi_1+\chi_7$	$c\chi_4-a\chi_6$	$c\chi_3+a\chi_5$
5	χ_5	$-\chi_6$	$-\chi_7$	$-\chi_8$	$b\chi_1$	$-b\chi_2$	$-b\chi_3$	$-b\chi_4$
6	χ_6	$-\chi_5$	$-\chi_8$	$-\chi_7$	$b\chi_2$	$-b\chi_1$	$b\chi_4$	$b\chi_3$
7	χ_7	χ_8	$-a\chi_5$	$a\chi_6$	$c\chi_5+b\chi_3$	$c\chi_6-b\chi_4$	$c\chi_7-ab\chi_1$	$c\chi_8-ab\chi_4$
8	χ_8	χ_7	$-a\chi_6$	$a\chi_5$	$c\chi_6-b\chi_4$	$c\chi_5+b\chi_3$	$c\chi_8-ab\chi_2$	$c\chi_7-ab\chi_1$

be expanded in the basis $\chi_k(1)$ from (3.26) as follows,

$$\tfrac{1}{4}\mathrm{Tr}_2\{\mathcal{K}_n\chi_k(2)\}=\sum_{m=1}^{8} C_{nk}^m\chi_m(1)\ , \tag{3.40}$$

where C_{nk}^m is a scalar coefficient. Appendix B works out the nonzero values of C_{nk}^m for the traces defined by Table IV and momenta as in (3.36)–(3.39). This procedure produces expansions for the four optical potentials U^{++}, U^{+-}, U^{-+}, and U^{--} in terms of the eight Dirac operators $\chi_m(1)$ as follows,

$$\hat{U}^{\rho_1'\rho_1}(\mathbf{p}',\mathbf{p})=\sum_{m=1}^{8} U_m^{\rho_1'\rho_1}(\mathbf{p}',\mathbf{p})\chi_m(1)\ , \tag{3.41}$$

where $U_m^{\rho_1'\rho_1}$ is a scalar function formed out of products of NN amplitudes, $\mathcal{M}_n^{\rho_1'\rho_2'\rho_1\rho_2}[a_1]$, nuclear form factors, $\rho_k^{\rho_2\rho_2'}(q)$, and kinematic factors C_{nk}^m of Appendix B,

$$U_m^{\rho_1'\rho_1}(\mathbf{p}',\mathbf{p})=-\sum_{\rho_2'\rho_2}\sum_{n=1}^{13}\sum_{k=1}^{4}\mathcal{M}_n^{\rho_1'\rho_2'\rho_1\rho_2}[a_1]\rho_k^{\rho_2\rho_2'}(q)C_{nk}^m\ . \tag{3.42}$$

It is useful to further expand the optical potential using the basis set $\chi_k(1)$. Combining Eqs. (3.22) and (3.41) yields

$$\hat{U}^{\rho_1'\rho_1}(\mathbf{p}',\mathbf{p})=\sum_{\rho_1'\rho_1}\sum_{m=1}^{8} U_m^{\rho_1'\rho_1}(\mathbf{p}',\mathbf{p}) \times\Lambda_1^{\rho_1'}(\mathbf{p}')\chi_m(1)\Lambda_1^{\rho_1}(\mathbf{p})\ , \tag{3.43}$$

where all the Dirac matrices are in the last three factors. In terms of the basis set $\chi_k(1)$, these may be written as follows:

$$\Lambda_1^{\rho_1'}(\mathbf{p}')\chi_m(1)\Lambda_1^{\rho_1}(\mathbf{p})=\sum_{n=1}^{8} D_{mn}^{\rho_1'\rho_1}\chi_n(1)\ . \tag{3.44}$$

Since the projection operators (3.2) are sums of coefficients times χ's, the group multiplication (3.27) can be used to deduce the matrix $D_{mn}^{\rho_1'\rho_1}$. We find

$$D_{mn}^{\rho_1'\rho_1}=\sum_{k=1}^{8}\left[\rho_1'\frac{E(\mathbf{p}')}{2m}\phi_{2mk}-\tfrac{1}{2}\rho_1'\phi_{6mk}+\tfrac{1}{2}\rho_1'\phi_{4mk}+\phi_{1mk}\right]\left[\rho_1\frac{E(\mathbf{p})}{2m}\phi_{k2n}-\tfrac{1}{2}\rho_1\phi_{k6n}+\tfrac{1}{2}\phi_{k1n}\right]\ . \tag{3.45}$$

Proceeding in this fashion, one obtains the desired expansion for the optical potential,

$$\hat{U}(\mathbf{p}',\mathbf{p})=\sum_{n=1}^{8} U_n(\mathbf{p}',\mathbf{p})\chi_n(1)\ , \tag{3.46}$$

where eight potentials U_n are defined by

$$U_n(\mathbf{p}',\mathbf{p})=\sum_{\rho_1'\rho_1}\sum_{m=1}^{8} U_m^{\rho_1'\rho_1}(\mathbf{p}',\mathbf{p})D_{mn}^{\rho_1'\rho_1},\quad n=1\text{–}8\ . \tag{3.47}$$

Introducing $\mathbf{p}_a=\frac{1}{2}(\mathbf{p}+\mathbf{p}')$ and $\mathbf{q}=\mathbf{p}-\mathbf{p}'$, and observing that $\chi_7(1)$ and $\chi_8(1)$ may be expressed as

$$\chi_7=\frac{\mathbf{p}_a\cdot\mathbf{q}}{m^2}+\frac{\mathbf{q}^2}{2m^2}-i\frac{\boldsymbol{\sigma}_1\cdot\mathbf{q}\times\mathbf{p}_a}{m^2}\ , \tag{3.48}$$

$$\chi_8=\gamma^0\left[\frac{\mathbf{p}_a\cdot\mathbf{q}}{m^2}+\frac{\mathbf{q}^2}{2m^2}-i\frac{\boldsymbol{\sigma}_1\cdot\mathbf{q}\times\mathbf{p}_a}{m^2}\right]\ , \tag{3.49}$$

the optical potential is finally rearranged to a form which proves convenient for later transformation to coordinate space:

$$\hat{U}(\mathbf{p}',\mathbf{p})=S+\gamma_1^0V-\frac{\boldsymbol{\alpha}_1\cdot\mathbf{q}}{m}T+\left[\frac{-E\gamma_1^0+\boldsymbol{\gamma}_1\cdot\mathbf{p}_a+m}{m}\right]C +\frac{\boldsymbol{\gamma}_1\cdot\mathbf{q}}{m}D+\frac{\boldsymbol{\alpha}_1\cdot\mathbf{p}_a}{m}F +i\frac{\boldsymbol{\sigma}_1\cdot\mathbf{q}\times\mathbf{p}_a}{m^2}(S_{LS}+\gamma_1^0V_{LS})\ , \tag{3.50}$$

where

$$S=U_1+\left[\frac{\mathbf{p}_a\cdot\mathbf{q}}{m^2}+\frac{\mathbf{q}^2}{2m^2}\right]U_7-U_6\ , \tag{3.51}$$

$$V = U_2 + \left[\frac{\mathbf{p}_a \cdot \mathbf{q}}{m^2} + \frac{\mathbf{q}^2}{2m^2} \right] U_8 + \frac{E}{m} U_6 \ , \tag{3.52}$$

$$T = U_3 + \tfrac{1}{2} U_5 \ , \tag{3.53}$$

$$C = U_6 \ , \tag{3.54}$$

$$D = U_4 + \tfrac{1}{2} U_6 \ , \tag{3.55}$$

$$F = U_5 \ , \tag{3.56}$$

$$S_{LS} = -U_7 \ , \tag{3.57}$$

$$V_{LS} = -U_8 \ . \tag{3.58}$$

Here, S is a Lorentz scalar potential, V is the time component of a vector potential, T is a tensor potential, C is a space-vector potential, D and F are potentials associated with time-reversal odd operators in (3.50), and S_{LS} and V_{LS} are scalar and vector spin-orbit potentials which directly enter the Dirac equation. When on-mass-shell NN amplitudes are used, as in this paper, time-reversal odd potentials D and F vanish. Thus six nonvanishing potentials contribute to the optical potential in this case. In general, these potentials depend on three rotational scalars formed out of momenta $\mathbf{p}$ and $\mathbf{p}'$, for example, $\mathbf{q}^2$, $\mathbf{p}_a^2$, and $\mathbf{q} \cdot \mathbf{p}_a$.

Equations (3.50)–(3.58) are the basic results of this section. They define the eight Dirac optical potentials. In order to calculate these potentials, one uses (3.4)–(3.15) to determine symmetrical NN amplitudes f_n^{ij}, Eqs. (3.19) and (3.21) to determine the Feynman amplitudes $\mathcal{M}_n^{\rho_1' \rho_2' \rho_1 \rho_2}[a_1]$ in all the ρ-spin sectors, and Eqs. (3.29)–(3.32) to determine the projected densities $\rho_k^{\rho_2' \rho_2}(q)$. These ingredients are combined in Eqs. (3.42) and (3.47) to determine eight optical potentials $U_1(\mathbf{p}', \mathbf{p})$ to $U_8(\mathbf{p}', \mathbf{p})$. Finally, Eqs. (3.50)–(3.58) determine the eight terms of the optical potential. Each potential depends on the energy and also is a nonlocal function of $\mathbf{p}$ and $\mathbf{p}'$.

Isospin effects are incorporated by a straightforward extension of the analysis. One executes the procedure twice, once with pp amplitudes and proton densities and once with pn amplitudes and neutron densities. The resulting proton and neutron contributions are added to form the optical potential as in (2.17).

If the potentials are functions only of $\mathbf{q}^2$ and the asymptotic momentum, $\hat{\mathbf{p}}$, or the energy E, they are equivalent to local potentials in coordinate space. This is obviously not true, in general. However, for high energy scattering a reasonably accurate local approximation may be obtained for each of the nonvanishing potentials.

IV. COORDINATE SPACE POTENTIAL

At sufficiently high energy, nucleon-nucleus elastic scattering becomes diffractive and very forward peaked. Consequently, the preponderance of experimental data is taken at relatively small angles. In such circumstances, a local form of the optical potential proves to be quite accurate. For example, the eikonal approximation is reasonably accurate for the experimentally observed angular range above 300 MeV,[26] and this involves the assumption that the momentum operator $\mathbf{p}$ stays near the asymptotic value $\hat{\mathbf{p}}$ throughout the scattering.[27] Similar approximations are used to obtain a local form for the potentials in Eqs. (3.51)–(3.58). The leading nonlocalities present in (3.50) due to $\boldsymbol{\alpha} \cdot \mathbf{q}/m$, $\boldsymbol{\gamma} \cdot \mathbf{p}_a/m$, and so on are treated exactly in coordinate space, but nonlocalities internal to the potentials S, V, and so on, are treated approximately.

Two main sources of nonlocality arise in the Dirac potentials. The first is due to momentum dependent covariants and projection operators. Assuming $\mathbf{p} \approx \hat{\mathbf{p}}$, nonlocal factors $E(\mathbf{p})$ and $E(\mathbf{p}')$ are replaced by $E = E(\hat{\mathbf{p}})$. Similarly, $\mathbf{p}/m \approx \hat{\mathbf{p}}/m$ and $\mathbf{p}_a \cdot \mathbf{q}/m = \frac{1}{2}(\mathbf{p}^2 - \mathbf{p}'^2)/m \approx 0$ are used to localize the matrix D in Eq. (3.45). These approximations are expected to be rather good at high energy since typical corrections involve

$$E(\mathbf{p}) \approx E + \frac{\mathbf{p}^2 - \hat{\mathbf{p}}^2}{2m} \approx E - \bar{V}_s \ , \tag{4.1}$$

where V_s is an average Schrödinger potential and the estimate is based on the WKB approximation, where $\mathbf{p}^2 = \hat{\mathbf{p}}^2 - 2mV_s$. Since $V_s \ll E$, it is a good approximation to simply use $E(\mathbf{p}) = E$. However, it must be noted that large angle scattering is more sensitive to nonlocalities and therefore the approximations work best at small momentum transfer.

The second source of nonlocality is the nucleon exchange contribution contained in the $\mathcal{M}_n^{ij}(u)$ NN amplitude terms of Eqs. (3.4)–(3.10). Direct terms, $\mathcal{M}_n(t)$, are naturally local since $t = -\mathbf{q}^2$, and they tend to be the most important contributions in p-nucleus scattering. Although intrinsically nonlocal, the exchange terms are much less important for small angle scattering at high energy. Care is nevertheless required. For on-mass-shell kinematics, $-u = 2mT_{\text{lab}} - \mathbf{q}^2$, where T_{lab} is the laboratory kinetic energy of the proton. Holding T_{lab} constant but allowing $\mathbf{q}^2$ to vary can give negative values of $-u$ for $\mathbf{q}^2$ beyond the physically allowed range for NN scattering in free space, but within the $\mathbf{q}^2$ range where the optical potential may be needed. As a result of this, localization of exchange based on $-u = 2mT_{\text{lab}} - \mathbf{q}^2$ is incorrect because it produces an unphysical singularity in the exchange terms of (3.4)–(3.15) when $\mu_m^2 + 2mT_{\text{lab}} - \mathbf{q}^2 = 0$.

Utilizing the Yukawa fits of NN amplitudes, a satisfactory approximation for nucleon exchange is obtained by following a prescription from nonrelativistic analyses. Exchange contributions are localized by replacing Yukawa denominators by the following angular averaged expression:

$$X_m(\hat{\mathbf{p}}^2, \mathbf{q}^2) = (4\pi)^{-1} \int d\Omega_{\text{p}} (\mu_m^2 - u)^{-1} (1 - u/\Lambda^2)^{-1} \ , \tag{4.2}$$

where

$$u = [E(\mathbf{p}) - E(\tfrac{1}{2}\mathbf{q})]^2 - (\mathbf{p} - \tfrac{1}{2}\mathbf{q})^2 \ .$$

Moreover, we replace $\mathbf{p}$ by $\hat{\mathbf{p}}$, in the spirit of the eikonal approximation. Then averaging over directions of $\hat{\mathbf{p}}$ yields functions of $\hat{\mathbf{p}}^2$ and $\mathbf{q}^2$, which are local. The localized exchange denominators are given by

$$X_m(\hat{\mathbf{p}}^2, \mathbf{q}^2) = \frac{\Lambda^2}{2\hat{p}q(\Lambda^2 - \mu_m)} \ln \left[\frac{(\Lambda^2 - u_-)(\mu_m^2 - u_+)}{(\Lambda^2 - u_+)(\mu_m^2 - u_-)} \right] \ , \tag{4.3}$$

where

$$u_+ = -(|\hat{\mathbf{p}}| + \tfrac{1}{2}|\mathbf{q}|)^2 + [E - E(\tfrac{1}{2}\mathbf{q})]^2 , \tag{4.4}$$

$$u_- = -(|\hat{\mathbf{p}}| - \tfrac{1}{2}|\mathbf{q}|)^2 + [E - E(\tfrac{1}{2}\mathbf{q})]^2 . \tag{4.5}$$

When each denominator $(\mu_m^2 - u)^{-1}(1-u/\Lambda^2)^{-1}$ is replaced by $X_m(\hat{\mathbf{p}}^2, \mathbf{q}^2)$, and kinematical factors are localized as discussed above, each of the potentials S, V, T, C, S_{LS}, and V_{LS} in Eqs. (3.51)–(3.58) becomes local and energy dependent. It is therefore possible to transform to coordinate space.

Consider the momentum space Dirac equation,

$$(\gamma^0 E - \boldsymbol{\gamma}\cdot\mathbf{p}' - m)\psi(\mathbf{p}') - (2\pi)^{-3}\int d^3p\, \hat{U}(\mathbf{p}',\mathbf{p})\psi(\mathbf{p}) = 0 , \tag{4.6}$$

where

$$\psi(\mathbf{p}') = \int d^3r\, e^{-i\mathbf{p}'\cdot\mathbf{r}}\psi(\mathbf{r}) , \tag{4.7}$$

and $U(\mathbf{p}',\mathbf{p})$ is given by the local form

$$\hat{U}(\mathbf{p}',\mathbf{p}) = S(q) + \gamma_1^0 V(q) - \frac{\boldsymbol{\alpha}_1\cdot\mathbf{q}}{m}T(q) + \left[\frac{-E\gamma_1^0 + \boldsymbol{\gamma}_1\cdot\mathbf{p}_a + m}{m}\right]C(q) + i\frac{\boldsymbol{\sigma}\cdot\mathbf{q}\times\mathbf{p}_a}{m^2}[S_{LS}(q) + \gamma_1^0 V_{LS}(q)] . \tag{4.8}$$

Energy dependence in each of the local potentials is implicit. Terms D and F are omitted since they vanish for the case under consideration. Combining (4.7) with (4.6) and integrating by parts produces

$$\int d^3r\, e^{-i\mathbf{p}'\cdot\mathbf{r}}(\gamma^0 E + i\boldsymbol{\gamma}\cdot\boldsymbol{\nabla} - m)\psi(\mathbf{r}) - (2\pi)^{-3}\int d^3p\, \hat{U}(\mathbf{p}',\mathbf{p})\int d^3r\, e^{i\mathbf{p}'\cdot\mathbf{r}}\psi(\mathbf{r}) . \tag{4.9}$$

Substitution of $\hat{U}$ and use of $\mathbf{p}\psi(\mathbf{r}) \to -i\boldsymbol{\nabla}\psi(\mathbf{r})$ and

$$\mathbf{p}_a\psi(\mathbf{r}) \to (-i\boldsymbol{\nabla} - \tfrac{1}{2}\mathbf{q})\psi(\mathbf{r})$$

leads to

$$(\gamma^0 E + i\boldsymbol{\gamma}\cdot\boldsymbol{\nabla} - m)\psi(\mathbf{r}) - (2\pi)^{-3}\int d^3q\, e^{-i\mathbf{q}\cdot\mathbf{r}} \times \left\{S(q) + \gamma^0 V(q) - \frac{\boldsymbol{\alpha}\cdot\mathbf{q}}{m}T(q) + [-E\gamma^0 + \boldsymbol{\gamma}\cdot(-i\boldsymbol{\nabla} - \tfrac{1}{2}\mathbf{q}) + m]C(q) + [S_{LS}(q) + \gamma_1^0 V_{LS}(q)]\frac{\boldsymbol{\sigma}\cdot\mathbf{q}\times\boldsymbol{\nabla}}{m^2}\right\}\psi(\mathbf{r}) , \tag{4.10}$$

where the $\mathbf{r}$ integration and a plane wave factor, $e^{-i\mathbf{p}'\cdot\mathbf{r}}$, are omitted. Moreover, the $\mathbf{p}$ integration at fixed $\mathbf{p}'$ has been converted to a $\mathbf{q}$ integration. Performing the $\mathbf{q}$ integration leads to

$$[\gamma^0 E + i\boldsymbol{\gamma}\cdot\boldsymbol{\nabla} - m - \hat{U}(\mathbf{r},\boldsymbol{\nabla})]\psi(\mathbf{r}) = 0 , \tag{4.11}$$

where

$$\hat{U}(\mathbf{r},\boldsymbol{\nabla}) = S(r) + \gamma^0 V(r) - i\frac{\boldsymbol{\alpha}\cdot\hat{\mathbf{r}}}{m}T'(r) + \frac{C(r)}{m}(-E\gamma^0 - i\boldsymbol{\gamma}\cdot\boldsymbol{\nabla} + m) - i\boldsymbol{\gamma}\cdot\boldsymbol{\nabla}\frac{C(r)}{2m} - [S'_{LS}(r) + \gamma^0 V'_{LS}(r)]\frac{\boldsymbol{\sigma}\cdot\mathbf{L}}{rm^2} , \tag{4.12}$$

and $\mathbf{L} = -i\mathbf{r}\times\boldsymbol{\nabla}$. Here,

$$S(r) = (2\pi)^{-3}\int d^3q\, e^{-i\mathbf{q}\cdot\mathbf{r}}S(q) , \tag{4.13}$$

and $V(r)$, $T(r)$, $C(r)$, $S_{LS}(r)$, and $V_{LS}(r)$ are obtained in exactly the same way from localized functions $V(q)$, $T(q)$, and so on, which appear in (4.8) and stem from Eqs. (3.51)–(3.58). A prime as in $T'(r)$ denotes $dT(r)/dr$, and similarly for S'_{LS} and V'_{LS}. These derivatives in coordinate space arise from $\mathbf{q}$ factors in momentum space and the fact that the localized potentials are spherically symmetric.

Although Eq. (4.13) may be solved directly, it is a little simpler to eliminate the $\boldsymbol{\gamma}\cdot\boldsymbol{\nabla}$ terms by the following transformation:

$$\psi(\mathbf{r}) = [1 + C(r)/m]^{-1/2}\tilde{\psi}(\mathbf{r}) . \tag{4.14}$$

One finds that $\tilde{\psi}(\mathbf{r})$ obeys the Dirac equation

$$[\gamma^0 E + i\boldsymbol{\gamma}\cdot\boldsymbol{\nabla} - m - \tilde{U}(\mathbf{r})]\tilde{\psi}(\mathbf{r}) = 0 \tag{4.15}$$

with a five term optical potential as follows:

$$\tilde{U}(r) = \tilde{S}(r) + \gamma^0\tilde{V}(r) - i\boldsymbol{\alpha}\cdot\hat{\mathbf{r}}\,\tilde{T}(r) - [\tilde{S}_{LS}(r) + \gamma^0\tilde{V}_{LS}(r)]\boldsymbol{\sigma}\cdot\mathbf{L} , \tag{4.16}$$

$$\tilde{S}(r) = S(r)/[1 + C(r)/m] , \tag{4.17}$$

$$\tilde{V}(r) = V(r)/[1 + C(r)/m] , \tag{4.18}$$

$$\tilde{T}(r) = T'(r)/[m + C(r)] , \tag{4.19}$$

$$\tilde{S}_{LS}(r) = S'_{LS}(r)/\{mr[m + C(r)]\} , \tag{4.20}$$

$$\tilde{V}_{LS}(r) = V'_{LS}(r)/\{mr[m + C(r)]\} . \tag{4.21}$$

Note that $C(r)$ does play a role in the scattering and therefore (4.16) represents the effects of six Dirac potentials. Since $\tilde{\psi} = \psi$ beyond the range of the potential $C(r)$, the same phase shifts are obtained from solving (4.11) or (4.15). Since Eq. (4.15) is simpler, our numerical calculations are based on this equation.

V. SCATTERING CALCULATIONS

Initial numerical calculations using the generalized impulse approximation, IA2 are based on complete sets of on-mass-shell amplitudes. Yukawa fits given in Ref. 16 together with symmetries determine all nonvanishing amplitudes of Eq. (3.1). Positive energy amplitudes are based on empirical phase shifts.[25] All other amplitudes are based on the meson exchange model. Nuclear form factors are

calculated from the wave functions of Horowitz and Serot[21] as in Eqs. (2.24)–(2.29). These ingredients are combined to provide a parameter-free specification of the Dirac optical potential. The essential point of the IA2 analysis is the use of complete sets of NN amplitudes based on a meson exchange dynamics. Negative energy couplings are predicted from a consistent set of meson-baryon couplings which give a good description of NN scattering in the energy region 0–1000 MeV. The analysis is logically simple in that a straightforward evaluation of $\hat{U} = -\frac{1}{4}\mathrm{Tr}_2\{\hat{\mathcal{M}}\hat{\rho}\}$ is involved.

Comparisons are made with the original form of the impulse approximation, IA1, in which five NN amplitudes are used. For IA1, the NN amplitude takes the form

$$\hat{F}(p_1p_2 \to p_1'p_2') = \sum_{k=1}^{5} f_k^{11}[a_1]\Gamma_k \tag{5.1}$$

in place of (3.1). The five NN amplitudes and five kinematic covariants in (5.1) are exactly the same as the first five terms of Eq. (3.3) for class 11 of the complete representation (3.1). This follows because these five amplitudes can be determined by positive energy matrix elements. However, it is a basic assumption that the five-term representation may be used on the complete Dirac space of two nucleons. IA1 is based on the ansatz that (5.1), without any projection operators, may provide an adequate representation of the NN amplitude in all ρ-spin sectors. As noted in Ref. 12, IA1 implicitly incorporates pseudoscalar πN coupling, as may be seen by expressing the one-pion-exchange amplitude in the form (5.1). IA2 replaces this ansatz with the prediction of a meson exchange model which explicitly incorporates pseudovector πN coupling.

Figures 3–5 show scalar, vector, and tensor potentials, $\tilde{S}$, $\tilde{V}$, and $\tilde{T}$ of (4.17)–(4.19), for 200 MeV proton scattering from ^{40}Ca. For the original impulse approximation based on the five-term NN amplitude, IA1, these are the only nonzero potentials. The figures show the IA1 results and the IA2 potentials based on the complete set of NN amplitudes. Although IA1 provides interesting predictions for spin observables in p-nucleus scattering in the 400–1000 MeV region, overly large scalar and vector potentials are predicted at low energy. The main reason for this is implicit incorporation of pseudoscalar πN coupling as discussed in Ref. 12. The meson ex-

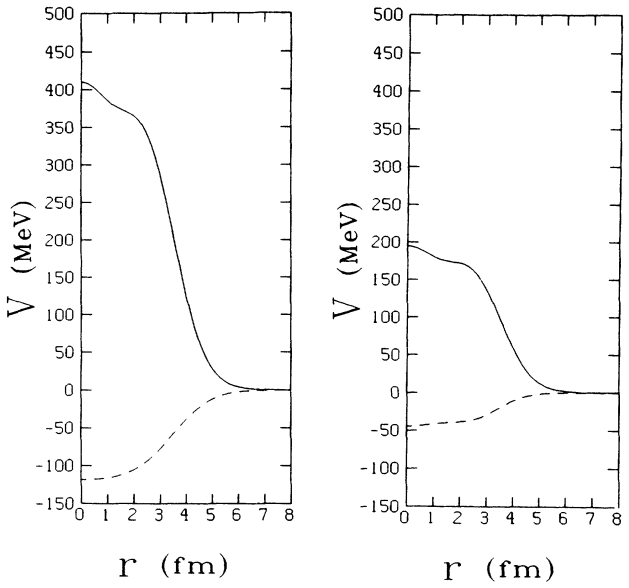

FIG. 4. Vector potential for ^{40}Ca. Solid line is real part and dashed line is imaginary part. Left-hand panel shows IA1 result and right-hand panel shows IA2 result.

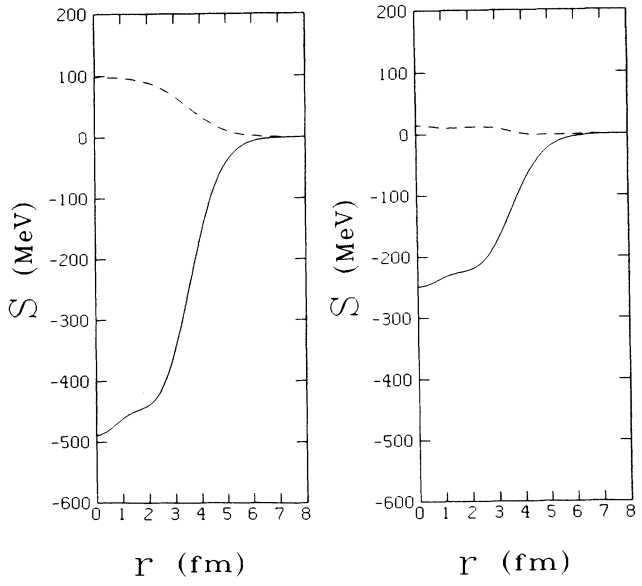

FIG. 3. Scalar potential for ^{40}Ca. Solid line is real part and dashed line is imaginary part. Left-hand panel shows IA1 result and right-hand panel shows IA2 result.

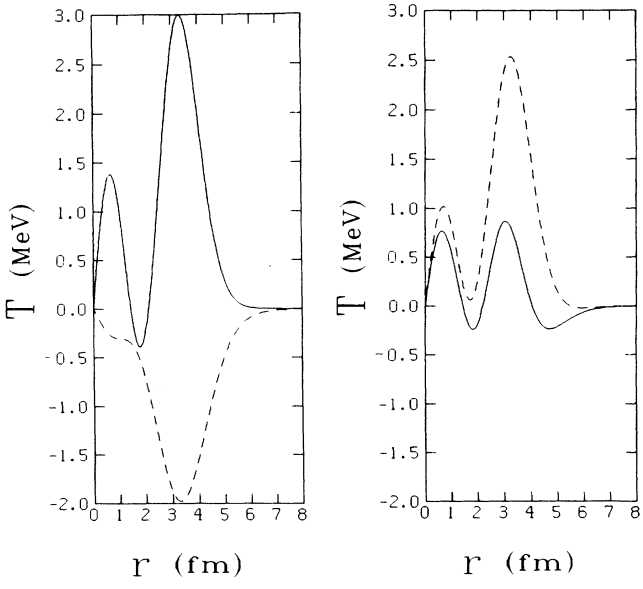

FIG. 5. Tensor potential for ^{40}Ca. Solid line is real part and dashed line is imaginary part. Left-hand panel shows IA1 result and right-hand panel shows IA2 result.

change model used as a basis for the generalized impulse approximation results in considerably smaller scalar and vector potentials at low energy. Figures 3 and 4 illustrate this difference at 200 MeV.

A second point is that IA2 determines six terms in the optical potential, although one of these is eliminated by the transformation (4.14). Figures 6–8 show the space-vector potential $C(r)$, the scalar spin-orbit potential $\tilde{S}_{LS}(r)$, and the vector spin-orbit potential $\tilde{V}_{LS}(r)$. The spin-orbit potentials which occur in the Dirac optical potential (4.16) should not be confused with the spin-orbit potential of the equivalent Schrödinger equation. The latter arises when the lower component of the Dirac wave function is eliminated to obtain a second order equation for the upper-component wave function. The large scalar and vector potentials of the Dirac equation provide the spin-orbit potential of the equivalent Schrödinger equation. In the generalized impulse approximation, the smaller scalar and vector potentials would seem to translate into a smaller spin-orbit term in the Schrödinger equation. However, this is not the whole story because the new spin-orbit terms, $\tilde{S}_{LS}$ and $\tilde{V}_{LS}$, also contribute.

Figures 9–14 show results for cross section, analyzing power, and spin rotation for elastic scattering of protons by ^{40}Ca at 200, 500, and 800 MeV, respectively. In each figure a solid line shows the result of the generalized impulse approximation, IA2, and a dashed line shows the result based on the original impulse approximation, IA1. Squares show experimental data. The main conclusion from these results is that the generalized impulse approximation provides a successful prediction of the experimental data over the 200–800 MeV energy range. At 200 MeV, the IA2 results are a significant improvement over the IA1 predictions and the agreement with data for spin observables is excellent. Theoretical cross sections at 200 MeV oscillate too much and this might be due to the influence of nucleon exchange contributions.

As noted above, the overly strong scalar and vector potentials in the IA1 approach at low energy are mainly an artifact of the implicit pseudoscalar pion coupling. Using a pseudovector covariant in place of Γ_5 in Eq. (5.1) produces scalar and vector strengths comparable to those of the IA2 approach. This is misleading, however. Detailed calculations for cross sections and spin observables, which will be reported in a future publication,

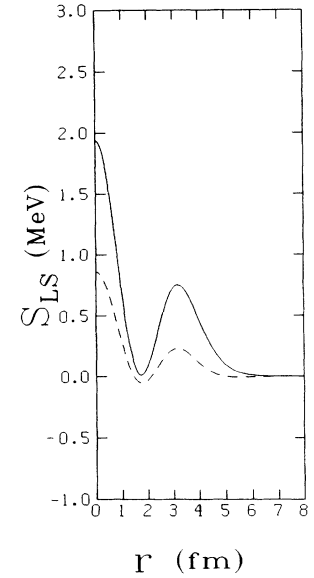

FIG. 7. Scalar spin-orbit potential for ^{40}Ca based on IA2. Solid line is real part and dashed line is imaginary part.

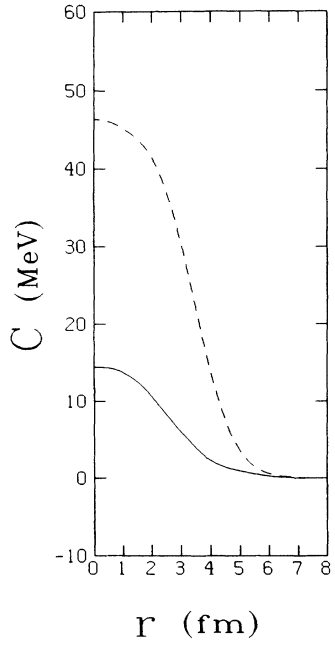

FIG. 6. Space-vector potential for ^{40}Ca based on IA2. Solid line is real part and dashed line is imaginary part.

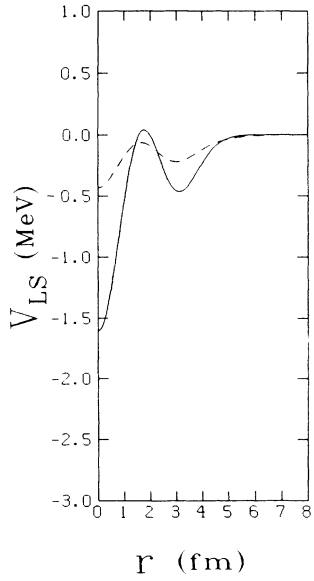

FIG. 8. Vector spin-orbit potential for ^{40}Ca based on IA2. Solid line is real part and dashed line is imaginary part.

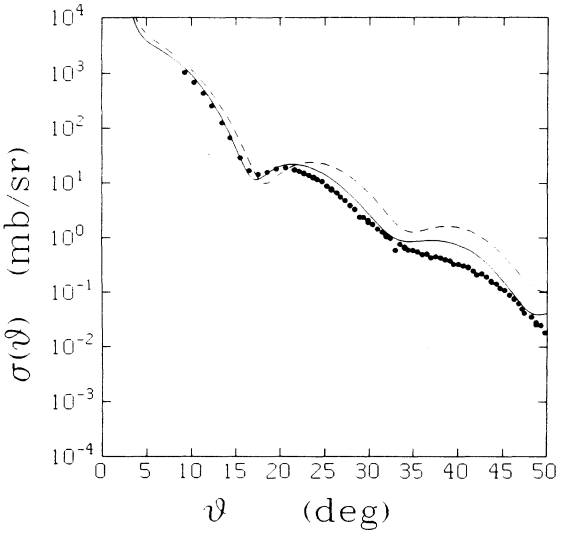

FIG. 9. Cross section for 200 MeV proton scattering by ^{40}Ca. Solid line shows IA2 result and dashed line shows IA1 result. Data from Refs. 28 and 29.

show that simple conversion of the pseudoscalar covariant to the pseudovector one in Eq. (5.1) yields results which are significantly different from, and inferior to, those of the full IA2 analysis. In fact, the various suggestions for accomplishing the conversion of pseudoscalar to pseudovector pion coupling do not agree well with each other. For example, the method suggested in Ref. 12 has been found to produce very poor results for proton scattering by ^{208}Pb even though it yields satisfactory results for ^{40}Ca and ^{16}O. These remarks illustrate that there is a serious ambiguity entailed in using less than a

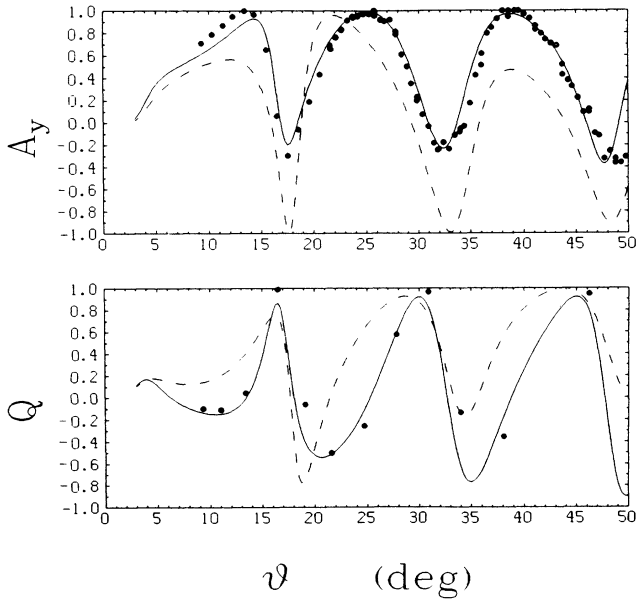

FIG. 10. Analyzing power (A_y) and spin rotation (Q) for 200 MeV proton scattering by ^{40}Ca. Solid line shows IA2 result and dashed line shows IA1 result. Data from Refs. 28 and 29.

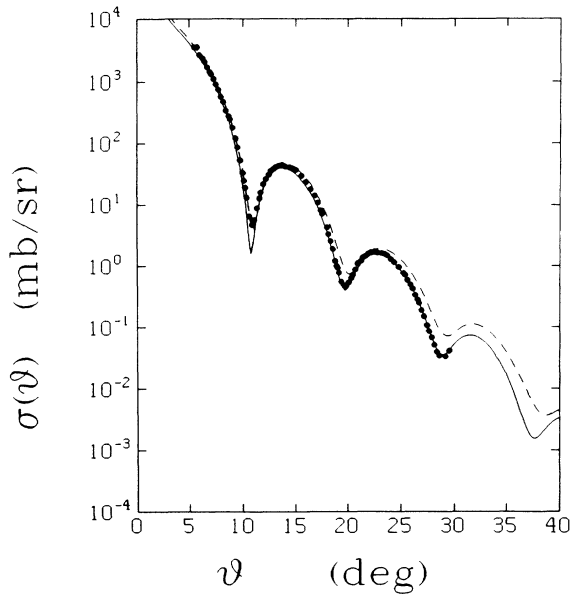

FIG. 11. Cross section for 500 MeV proton scattering by ^{40}Ca. Solid line shows IA2 result and dashed line shows IA1 result. Data from Ref. 5.

complete set of NN amplitudes to extend the NN interaction to the full Dirac space of two nucleons.

At 500 MeV the theoretical cross section based on IA2 is very good and the spin observables are also good, although somewhat less so than for the original impulse approximation, IA1. At 800 MeV, theoretical predictions based on IA2 are again in rather good agreement with ex-

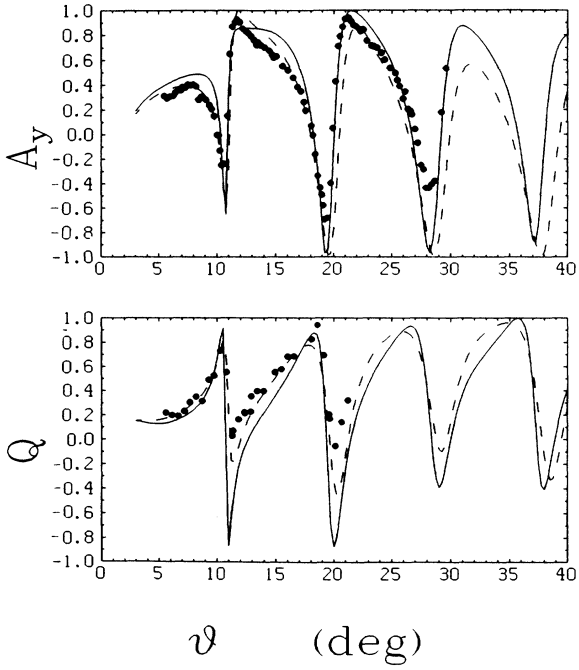

FIG. 12. Analyzing power (A_y) and spin rotation (Q) for 500 MeV proton scattering by ^{40}Ca. Solid line shows IA2 result and dashed line shows IA1 result. Data from Refs. 5 and 30.

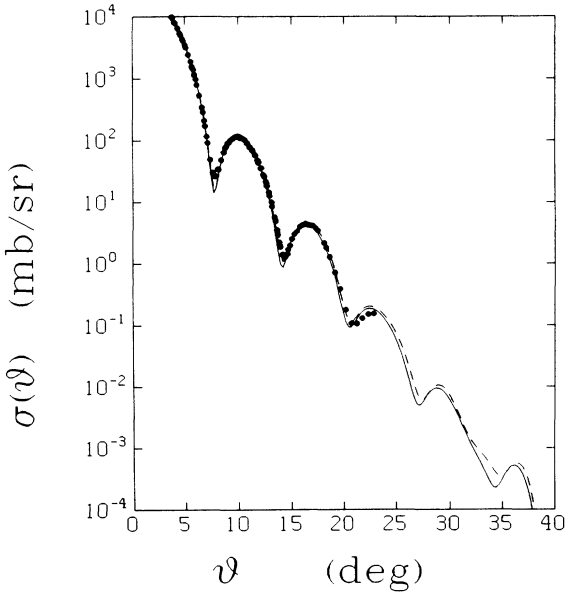

FIG. 13. Cross section for 800 MeV proton scattering by ^{40}Ca. Solid line shows IA2 result and dashed line shows IA1 result. Data from Ref. 7.

perimental data. The differences between the IA1 and IA2 results at 500 and 800 MeV are due to the somewhat weaker scalar and vector strengths obtained for IA2. We have observed that the results are quite sensitive to the rather small difference $\rho_{LC}=\rho_V-\rho_S$ due to the lower components of the Dirac Hartree wave functions. For example, fixing ρ_V and doubling the lower component density ρ_{LC} brings the IA2 results into very good agreement with the data. The variation of the scalar density is about 2% when ρ_{LC} is doubled. Enhancement of the scalar-vector difference arises naturally from vacuum polarization corrections to the mean field theory of quantum hadrodynamics. A future article will analyze proton scattering observables at 500 and 800 MeV including the vacuum polarization correction.

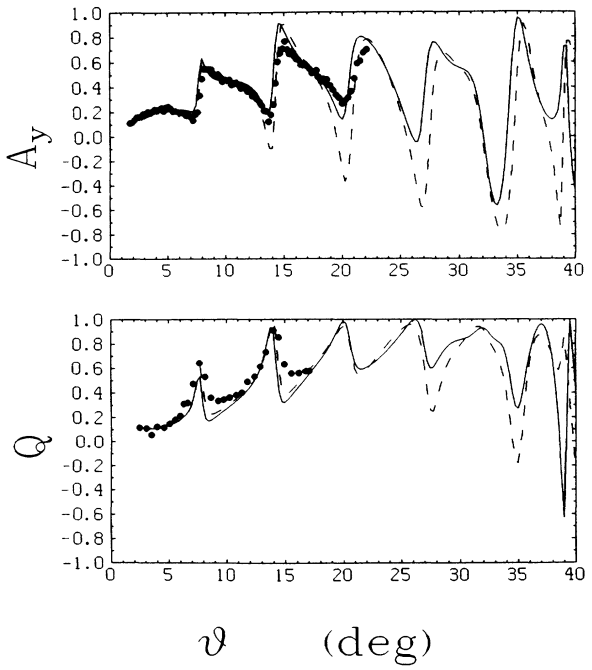

FIG. 14. Analyzing power (A_y) and spin rotation (Q) for 800 MeV proton scattering by ^{40}Ca. Solid line shows IA2 result and dashed line shows IA1 result. Data from Ref. 7.

Because of the reduced scalar and vector potentials at low energy in the IA2 approach, there is an apparent mismatch between the low energy optical potential and the mean field used to calculate Dirac-Hartree wave functions. The latter involves a 400 MeV scalar potential and a 300 MeV vector potential in the nuclear interior. This raises the interesting question whether the NN interaction of the IA2 approach implies significantly different nuclear wave functions and densities in a self-consistent analysis. There is a related possibility that improved nuclear wave functions could alter the predictions for proton scattering. A self-consistent analysis of nuclear wave functions and optical potentials using the meson theoretical NN interaction is far beyond the scope of the present work, but the desirability of such an analysis is noted.

VI. SUMMARY

Utilizing a Yukawa representation of a complete set of Lorentz invariant NN amplitudes,[16] the impulse approximation optical potential for use in the Dirac equation is constructed in this paper. Nuclear wave functions used in the construction are obtained from the Dirac-Hartree calculations of Horowitz and Serot.[21] The first order optical potential $\hat{U}$ is expressed as $\hat{U}=-\frac{1}{4}\mathrm{Tr}_2\{\hat{\mathcal{M}}\hat{\rho}\}$, where $\hat{\mathcal{M}}$ is the Feynman amplitude for NN scattering and $\hat{\rho}$ is the relativistic nuclear density matrix. This is the relativistic analog of the $t\rho$ impulse approximation. Effects of the nuclear medium on the NN amplitudes are not considered, nor are double scattering corrections to the optical potential included. Moreover, a factorized form of the optical potential is used in which dependence of the NN amplitudes on the Fermi motion of the nucleons in the nucleus is neglected.

Because $\hat{U}$ contains effects of coupling to negative energy states, it is essential to use a complete set of NN amplitudes in order to avoid ambiguities in the construction. In principle, there are 56 independent NN amplitudes for each isospin state. For on-mass-shell kinematics, as are used in this paper, 44 amplitudes suffice. Attempts to describe the NN amplitude by fewer terms are not well founded, even though IA1, which uses five terms, has proved successful in describing p-nucleus data at intermediate energy. Some improvement of the five-term impulse approximation is possible by converting the pseudoscalar covariant to a pseudovector one.[12,14] This prescription is ambiguous and our results to be reported in a future article show that it is not an adequate substitute for the complete IA2 analysis. Therefore a meson exchange model must be adopted as in this paper to extend the available NN data to negative energy sectors of the full Dirac space of two nucleons. Previous work

developed suitable sets of kinematical covariants which form a linearly independent basis for expansion of the NN amplitudes. In this work, we use the kinematical covariants of Ref. 16 since it is desirable to effect a separation of direct and exchange terms in the NN amplitude in order to treat properly exchange contributions to the optical potential. For high energy scattering, a simpler representation given in Ref. 15 may also be used. For either case, this paper provides the analysis necessary to construct the optical potential.

The optical potential is first formulated in momentum space using the Yukawa fits of Lorentz invariant amplitudes. The Feynman NN amplitudes contain separate direct and exchange terms such that antisymmetry is incorporated explicitly and simply. It is found that the factorized optical potential, using on-mass-shell NN amplitudes, contains six terms. In order to perform calculations in coordinate space, nucleon exchange contributions to the optical potential are localized as in Eq. (4.2). Additionally, where off-shell momenta occur, they are replaced by on-shell momenta in the spirit of the eikonal approximation. However, leading nonlocalities of the optical potential are retained as these may be treated exactly in coordinate space. An equivalent five term optical potential is obtained by transforming the coordinate space wave function as in (4.14). Each of the potentials has been calculated and the steps involved in carrying out the analysis form the bulk of this paper.

Some initial calculations for proton-nucleus scattering have been carried out and the results exhibit good agreement with experimental data for p-^{40}Ca scattering at 200, 500, and 800 MeV. There are no variable parameters in the calculations. Given the formalism of this paper, it is a straightforward matter to extend the calculations to explore more fully the systematics of the IA2 impulse approximation. A future article will do so.

A main conclusion of the present work is that ambiguities in the construction of the Dirac optical potential may be eliminated by use of complete sets of NN amplitudes based on the meson exchange model of the nuclear force.[28] The meson exchange model adopted in this work[18–20] uses coupling constants and cutoffs which are typical of other boson-exchange models[29] and are similar to those of the quantum hadrodynamics model of Serot and Walecka,[30] and the relativistic Breuckner-Hartree-Fock approaches of Anastasio, Celenza, and Shakin[31] and Brockmann and Machleidt.[32] We do not expect a large model dependence of the results since the constraint of describing the NN data over a broad energy range is rather restrictive. A point deserving further study, however, is the role of the pion. Since the impulse approximation includes Fock terms due to exchange, the pion plays a significant role. This is in contrast to the Hartree model of nuclear wave functions where the pion plays no role.

An objective of this work was to incorporate the pseudovector πN coupling in a consistent fashion in order to obtain reasonable potentials at low energy. This objective was met by basing the IA2 analysis on the relativistic meson exchange model of van Faassen and Tjon. The characteristic Dirac improvement in the description of spin observables for proton-nucleus scattering is obtained with significantly smaller scalar and vector potentials at low energy in the IA2 approach. The meson exchange model is very similar to models which are used commonly to calculate meson exchange currents in electromagnetic reactions. Therefore the IA2 analysis tends to unify the theoretical analysis of proton scattering with that of NN scattering and meson exchange currents. Virtual pair effects are included implicitly when one solves the Dirac equation and these are given a foundation similar to that which exists for pair currents in electromagnetic reactions.

ACKNOWLEDGMENTS

One of us (J.A.T.) acknowledges the hospitality of the Nuclear Theory Group at the University of Maryland. Support of the University of Maryland Center for Intensive Computation for computer calculations is gratefully acknowledged. The support of the U.S. Department of Energy for this work is gratefully acknowledged.

APPENDIX A: DIRAC-HARTREE DENSITY

In the Dirac-Hartree approach to the nuclear shell model, each single particle orbital is a solution of the Dirac equation with scalar and vector potentials. Potentials are determined self-consistently from the nuclear density and meson exchange interactions treated in the mean-field approximation. Quantum numbers n (radial), l (orbital angular momentum), j (total angular momentum), μ (z component of total angular momentum), and t (isospin projection) characterize a given orbital. The Dirac wave function takes the form

$$\psi_{njl\mu t}(\mathbf{r})=i\begin{bmatrix} G_{nljt}(r) \\ -i\sigma_r F_{njlt}(r)\end{bmatrix} Y^{\mu}_{lj}(\hat{\mathbf{r}}) , \tag{A1}$$

where angular eigenfunctions of good j and $l=j\pm\frac{1}{2}$ are formed out of spherical harmonics, $Y_{lm}(\hat{\mathbf{r}})$, Pauli spinors, χ_s, and Clebsch-Gordan coefficients,

$$Y^{\mu}_{lj}(\hat{\mathbf{r}})=\sum_{m,s}\langle l\, m\, \tfrac{1}{2}\, s \mid j\,\mu\rangle Y_{lm}(\hat{\mathbf{r}})\chi_s . \tag{A2}$$

Sums over s range from $-\frac{1}{2}$ to $+\frac{1}{2}$ and sums over m range from $-l$ to $+l$.

For a closed-shell nucleus, each of the $2j+1$ magnetic substates is occupied and the nuclear density matrix of Eq. (2.22) is

$$\hat{\rho}(\mathbf{r})=4\sum_{njlt}\sum_{\mu=-j}^{j}\psi_{njl\mu t}(\mathbf{r})\bar{\psi}_{njl\mu t}(\mathbf{r})=4\sum_{njlt}\begin{bmatrix} G_{nljt}(r) \\ -i\sigma_r F_{njlt}(r)\end{bmatrix}\sum_{s,s'}A_{ss'}\chi_s\chi^{\dagger}_{s'}[G_{nljt}(r),\ -i\sigma_r F_{njlt}(r)] , \tag{A3}$$

where $A_{ss'}$ is a 2×2 matrix defined as follows,

$$\sum_{\mu=-j}^{j} Y_{lj}^{\mu}(\hat{\mathbf{r}})Y_{lj}^{\mu}(\hat{\mathbf{r}})^{\dagger}=\sum_{s,s'} A_{ss'}\chi_s\chi_{s'}^{\dagger} . \tag{A4}$$

Radial wave functions are real in the Dirac-Hartree analysis. The matrix A may be written as

$$A_{ss'}=\sum_{\mu,m,m'} \langle lm\ \tfrac{1}{2}s\ |\ j\mu\rangle\langle lm'\ \tfrac{1}{2}s'\ |\ j\mu\rangle Y_{lm}^{*}(\hat{\mathbf{r}})Y_{lm'}(\hat{\mathbf{r}}) . \tag{A5}$$

An alternative form is obtained by the substitutions $m\rightarrow -m'$, $m'\rightarrow -m$, and $\mu\rightarrow -\mu$ as follows,

$$A_{ss'}=\sum_{\mu,m,m'} (-1)^{m-m'}\langle lm\ \tfrac{1}{2}-s\ |\ j\mu\rangle\langle lm'\ \tfrac{1}{2}-s'\ |\ j\mu\rangle \times Y_{lm}^{*}(\hat{\mathbf{r}})Y_{lm'}(\hat{\mathbf{r}}) , \tag{A6}$$

after the reflection properties of the Clebsch-Gordan coefficients and the spherical harmonics are taken into account. In (A5), $m=\mu-s$ and $m'=\mu-s'$, since otherwise the Clebsch-Gordan coefficients vanish. Similarly, in (A6), $m=\mu+s$ and $m'=\mu+s'$. Comparing (A5) and (A6), one sees that $A_{s,s'}$ must vanish when $s'=-s$ since then $(-1)^{m-m'}=-1$ and there is a term in (A6) equal and opposite to each term in (A5). Moreover, when $s'=s$, it follows that $m=m'$ and the average of (A5) and (A6) can be written as follows:

$$A_{ss}=\tfrac{1}{2}\sum_{m}(\langle lm\ \tfrac{1}{2}\ \tfrac{1}{2}\ |\ j\ m\ +\tfrac{1}{2}\rangle^2 + \langle lm\ \tfrac{1}{2}\ -\tfrac{1}{2}\ |\ j\ m\ -\tfrac{1}{2}\rangle^2)\ |\ Y_{lm}(\hat{\mathbf{r}})\ |^2 . \tag{A7}$$

The Clebsch-Gordan coefficients are elementary. For $j=l\pm\frac{1}{2}$, we find

$$A_{ss}=\tfrac{1}{2}\sum_{m}\left[\frac{j+\frac{1}{2}\pm m}{2l+1}+\frac{j+\frac{1}{2}\mp m}{2l+1}\right]\ |\ Y_{lm}(\hat{\mathbf{r}})\ |^2 , \tag{A8}$$

and terms involving m obviously cancel. By use of

$$\sum_{m}\ |\ Y_{lm}(\hat{\mathbf{r}})\ |^2=\frac{2l+1}{4\pi} , \tag{A9}$$

the sum is evaluated to be

$$A_{ss'}=\delta_{ss'}\frac{j+\frac{1}{2}}{4\pi} . \tag{A10}$$

Substitution into (A3) then yields

$$\sum_{\mu=-j}^{j} Y_{lj}^{\mu}(\hat{\mathbf{r}})Y_{lj}^{\mu}(\hat{\mathbf{r}})^{\dagger}=\frac{j+\frac{1}{2}}{4\pi}\mathbf{1} , \tag{A11}$$

where $\mathbf{1}$ represents the unit operator in the Pauli-spin space. Consequently, the Dirac-Hartree density for a closed shell nucleus takes the form of a 4×4 matrix as follows,

$$\hat{\rho}(\mathbf{r})=4\sum_{nljt}\begin{bmatrix} [G_{nljt}(r)]^2\mathbf{1} & -i\sigma_r G_{nljt}(r)F_{nljt}(r) \\ -i\sigma_r G_{nljt}(r)F_{nljt}(r) & -[F_{nljt}(r)]^2\mathbf{1}\end{bmatrix} . \tag{A12}$$

Equivalently, this may be expressed in terms of Dirac matrices

$$\hat{\rho}(\mathbf{r})=\rho_S(r)+\gamma_2^0\rho_V(r)-\tfrac{1}{2}i\boldsymbol{\alpha}_2\cdot\hat{\mathbf{r}}\rho_T(r) , \tag{A13}$$

where scalar, vector, and tensor densities are given by Eqs. (2.27)–(2.29) of the text. Fourier transformation as in (2.21) produces scalar, vector, and tensor nucleus form factors,

$$\hat{\rho}(\mathbf{q})=\int d^3r[\rho_S(r)+\gamma_2^0\rho_V(r)-(2r)^{-1}\rho_T\boldsymbol{\alpha}_2\cdot\nabla_q]e^{i\mathbf{q}\cdot\mathbf{r}} =\rho_S(q)+\gamma_2^0\rho_V(q)-(2m)^{-1}\boldsymbol{\alpha}_2\cdot\mathbf{q}\rho_T(q) , \tag{A14}$$

where scalar, vector, and tensor form factors are defined as in Eqs. (2.24)–(2.26).

APPENDIX B

Traces needed for construction of the optical potential involve the kinematic covariants $\mathcal{K}_n$, $n=1-13$, as defined in Table II, and the set of parity invariant Dirac matrices χ_k defined in Eq. (3.26). For the covariants $\mathcal{K}_1$ to $\mathcal{K}_9$, which do not involve the Fierz exchange operator $\tilde{S}$, these traces can be all evaluated in terms of three elementary traces as follows,

$$\tfrac{1}{4}\mathrm{Tr}_2\{\mathcal{K}_n\}=\delta_{n1}+\delta_{n7},\quad n=1-9 \tag{B1}$$

$$\tfrac{1}{4}\mathrm{Tr}_2\{\mathcal{K}_n\gamma_2^{\mu}\}=\gamma_1^{\mu}\delta_{n2}+Q_{11}^{\mu}\delta_{n6},\quad n=1-9 \tag{B2}$$

$$\tfrac{1}{4}\mathrm{Tr}_2\{\mathcal{K}_n\boldsymbol{\alpha}_2\}=2\boldsymbol{\alpha}_1\delta_{n3},\quad n=1-9 . \tag{B3}$$

The remaining covariants $\mathcal{K}_{10}$ to $\mathcal{K}_{13}$ do involve the Fierz exchange operator $\tilde{S}$ and these may be evaluated most easily by use of the exchange property

$$\gamma_2^{\mu}\tilde{S}=\gamma_1^{\mu}\tilde{S} , \tag{B4}$$

which follows from the definition of $\tilde{S}$, i.e.,

$$\tilde{S}_{\alpha\beta,\alpha'\beta'}=\delta_{\alpha\beta'}\delta_{\beta\alpha'} , \tag{B5}$$

where α and β are Dirac indices for particle 1 while α' and β' are Dirac indices for particle 2. An explicit representation of $\tilde{S}$ in terms of Fermi covariants is[10,12]

$$\tilde{S}=\tfrac{1}{4}(\mathcal{K}_1+\mathcal{K}_2+\tfrac{1}{2}\mathcal{K}_3+\mathcal{K}_4+\mathcal{K}_5) . \tag{B6}$$

It follows from (B6) that

$$\tfrac{1}{4}\mathrm{Tr}_s\{\tilde{S}\}=\tfrac{1}{4} . \tag{B7}$$

For covariant $\mathcal{K}_{10}$ these properties of $\tilde{S}$ lead to the following results for the traces which appear in Eq. (3.35):

$$\begin{aligned}\tfrac{1}{4}\mathrm{Tr}_2\{\mathcal{K}_{10}\chi_k(2)\}&=\tfrac{1}{4}\mathrm{Tr}_2\{\gamma_2\cdot Q_{12}\tilde{S}\chi_k(2)\}\\ &=\tfrac{1}{4}\mathrm{Tr}_2\{\chi_k(2)\gamma_2\cdot Q_{12}\tilde{S}\}\\ &=\tfrac{1}{4}\mathrm{Tr}_2\{\tilde{S}\chi_k(1)\gamma_1\cdot Q_{12}\}\\ &=\tfrac{1}{4}\mathrm{Tr}_2\{\tilde{S}\}\chi_k(1)\gamma_1\cdot Q_{12}\\ &=\tfrac{1}{4}\chi_k(1)\gamma_1\cdot Q_{12} .\end{aligned} \tag{B8}$$

In the second line, invariance of a trace with respect to cyclic permutations of $\chi_k(2)$ has been used to move $\chi_k(2)$ to the left-hand side. Note that $\chi_k(2)$ involves only Dirac matrices for particle 2. Next, the commuta-

tion rule (B4) is used to commute $\tilde{S}$ to the left, thereby changing Dirac matrices for particle 2 into Dirac matrices for particle 1. This accounts for the appearance of $\chi_k(1)$. Finally, the Dirac matrices for particle 1 are taken out of the trace since they are not affected by the sum over Dirac indices of particle 2. The only trace actually needed is given by (B7). From this example, one may appreciate that Dirac traces involving $\tilde{S}$ are elementary due to (B4).

A similar analysis for covariant $\mathcal{H}_{11}$ produces

$$\begin{aligned}\tfrac{1}{4}\mathrm{Tr}_2\{\mathcal{H}_{11}\chi_k(2)\}&=\tfrac{1}{4}\mathrm{Tr}_2\{\gamma_1\cdot Q_{21}\tilde{S}\chi_k(2)\}\\&=\gamma_1\cdot Q_{21}\chi_k(1)\tfrac{1}{4}\mathrm{Tr}_2\{\tilde{S}\}\\&=\tfrac{1}{4}\gamma_1\cdot Q_{21}\chi_k(1)\ .\end{aligned}\tag{B9}$$

The analysis for covariants $\mathcal{H}_{12}$ and $\mathcal{H}_{13}$ differs only due to the presence of $P=\gamma_1^5\gamma_2^5$. We find the following results:

$$\begin{aligned}\tfrac{1}{4}\mathrm{Tr}_2\{\mathcal{H}_{12}\chi_k(2)\}&=\gamma_1^5\tfrac{1}{4}\mathrm{Tr}_2\{\gamma_2^5\gamma_2\cdot Q_{12}\tilde{S}\chi_k(2)\}\\&=\tfrac{1}{4}\gamma_1^5\chi_k(1)\gamma_1^5\gamma_1\cdot Q_{12}\ ,\end{aligned}\tag{B10}$$

$$\begin{aligned}\tfrac{1}{4}\mathrm{Tr}_2\{\mathcal{H}_{13}\chi_k(2)\}&=\gamma_1^5\tfrac{1}{4}\mathrm{Tr}_2\{\gamma_2^5\gamma_1\cdot Q_{21}\tilde{S}\chi_k(2)\}\\&=\tfrac{1}{4}\gamma_1^5\gamma_1\cdot Q_{12}\chi_k(1)\gamma_1^5\ .\end{aligned}\tag{B11}$$

Since γ^5 anticommutes with γ^μ, and $(\gamma^5)^2=1$, (B11) may be rewritten as

$$\tfrac{1}{4}\mathrm{Tr}_2\{\mathcal{H}_{13}\chi_k(2)\}=-\tfrac{1}{4}\gamma_1\cdot Q_{12}\gamma_1^5\chi_k(1)\gamma_1^5\ .\tag{B12}$$

Finally, the γ^5 matrices in (B10) and (B12) are eliminated by noting that

$$\begin{aligned}\gamma^5\chi_k\gamma^5&=\{\chi_1,-\chi_2,\chi_3,-\chi_4,\chi_5,-\chi_6,\chi_7,-\chi_8\}\\&=(-1)^{k+1}\chi_k\ .\end{aligned}\tag{B13}$$

Therefore we find

$$\tfrac{1}{4}\mathrm{Tr}_2\{\mathcal{H}_2\chi_k(2)\}=(-1)^{k+1}\tfrac{1}{4}\mathrm{Tr}_2\{\mathcal{H}_{10}\chi_k(2)\}\ ,\tag{B14}$$

$$\tfrac{1}{4}\mathrm{Tr}_2\{\mathcal{H}_{13}\chi_k(2)\}=(-1)^{k+1}\tfrac{1}{4}\mathrm{Tr}_2\{\mathcal{H}_{11}\chi_k(2)\}\ .\tag{B15}$$

A summary of the nonzero traces obtained in this fashion is given in Table IV of the text.

Each trace over particle 2 indices produces a matrix in the particle 1 Dirac space. These matrices are expanded in the basis $\chi_k(1)$ of Eq. (3.26) as follows,

$$\tfrac{1}{4}\mathrm{Tr}_2\{\mathcal{H}_n\chi_k(2)\}=\sum_{m=1}^{8}C_{n,k}^m\chi_m(1)\ .\tag{B16}$$

Results for covariants $\mathcal{H}_1$ to $\mathcal{H}_9$ can be read from Table III and Eqs. (3.26) and (3.27). We find

$$C_{1,1}^1=1,\quad C_{2,2}^2=1,\quad C_{2,4}^4=1,\quad C_{3,3}^3=2\ ,$$

$$C_{6,2}^1=\frac{E(\mathbf{p})+E(\mathbf{p}')}{2m},\quad C_{6,4}^1=\frac{2\mathbf{q}\cdot\mathbf{p}-\mathbf{q}^2}{2m},\quad C_{7,1}^2=\frac{E(\frac{1}{2}\mathbf{q})}{m}\ ,$$

to be the only nonzero value of C_{nk}^m for $n=1$–9. Covariants $\mathcal{H}_{10}$ and $\mathcal{H}_{11}$ produce more complicated forms. A straightforward analysis leads to the following results:

$$C_{10,1}^2=\frac{E(\mathbf{p}')+E(\frac{1}{2}\mathbf{q})}{8m},\quad C_{10,1}^6=-\tfrac{1}{8},\quad C_{10,1}^4=\tfrac{3}{16}\ ,$$

$$C_{11,1}^2=\frac{E(\mathbf{p})+E(\frac{1}{2}\mathbf{q})}{8m},\quad C_{11,1}^6=-\tfrac{1}{8},\quad C_{11,1}^4=-\tfrac{1}{16}\ ,$$

$$C_{10,2}^1=\frac{E(\mathbf{p}')+E(\frac{1}{2}\mathbf{q})}{8m},\quad C_{10,2}^5=-\tfrac{1}{8},\quad C_{10,2}^3=-\tfrac{3}{16}\ ,$$

$$C_{11,2}^1=\frac{E(\mathbf{p})+E(\frac{1}{2}\mathbf{q})}{8m},\quad C_{11,2}^5=\tfrac{1}{8},\quad C_{11,2}^3=-\tfrac{1}{16}\ ,$$

$$C_{10,3}^4=\frac{E(\mathbf{p}')+E(\frac{1}{2}\mathbf{q})}{8m},\quad C_{10,3}^2=\frac{-2\mathbf{q}\cdot\mathbf{p}+\frac{3}{2}\mathbf{q}^2}{8m^2},\quad C_{10,3}^8=\tfrac{1}{8}\ ,$$

$$C_{11,3}^4=\frac{-E(\mathbf{p})-E(\frac{1}{2}\mathbf{q})}{8m},\quad C_{11,3}^8=\tfrac{1}{8},\quad C_{11,3}^2=\frac{1}{16}\frac{\mathbf{q}^2}{m^2}\ ,$$

$$C_{10,4}^3=\frac{E(\mathbf{p}')+E(\frac{1}{2}\mathbf{q})}{8m},\quad C_{10,4}^7=-\tfrac{1}{8},\quad C_{10,4}^1=\frac{2\mathbf{q}\cdot\mathbf{p}-\frac{3}{2}\mathbf{q}^2}{8m^2},$$

$$C_{11,4}^3=\frac{-E(\mathbf{p})-E(\frac{1}{2}\mathbf{q})}{8m},\quad C_{11,4}^7=\tfrac{1}{8},\quad C_{11,4}^1=\frac{1}{16}\frac{\mathbf{q}^2}{m^2}\ .$$

The coefficients $C_{n,k}^m$ for covariants $\mathcal{H}_{12}$ and $\mathcal{H}_{13}$ are obtained from those given above by the rule, stemming from (B14) and (B15),

$$C_{12,k}^m=(-1)^{k+1}C_{10,k}^m\ ,$$

$$C_{13,k}^m=(-1)^kC_{11,k}^m\ .$$

If a nonzero value of $C_{n,k}^m$ is not determined by these equations, then $C_{n,k}^m=0$ is the correct value.

[1]J. A. McNeil, J. R. Shepard, and S. J. Wallace, Phys. Rev. Lett. **50**, 1439 (1983).

[2]L. G. Arnold, B. C. Clark, R. L. Mercer, D. G. Ravenhall, and A. M. Saperstein, Phys. Rev. C **19**, 917 (1979); B. C. Clark, R. L. Mercer, and P. Schwandt, Phys. Lett. **122B**, 211 (1983); B. C. Clark, S. Hama, and R. L. Mercer, in *The Interaction Between Medium Energy Nucleons in Nuclei—1982,* Proceedings of the Workshop held at Indiana University, Bloomington, 1982, edited by H. O. Meyer (AIP, New York, 1983), p. 260 (AIP Conf. Proc. No. 97).

[3]J. R. Shepard, J. A. McNeil, and S. J. Wallace, Phys. Rev. Lett. **50**, 1443 (1983).

[4]B. C. Clark, S. Hama, R. L. Mercer, L. Ray, and B. D. Serot, Phys. Rev. Lett. **50**, 1644 (1983).

[5]G. W. Hoffmann, L. Ray, M. L. Bartlett, R. Fergerson, J. McGill, E. C. Milner, K. K. Seth, D. Barlow, M. Bosko, S. Iverson, M. Kaletka, A. Saha, and D. Smith, Phys. Rev. Lett. **47**, 1436 (1981).

[6]B. C. Clark, S. Hama, R. L. Mercer, L. Ray, G. W. Hoffman, and B. D. Serot, Phys. Rev. C **28**, 1421 (1983).

[7]L. Ray and G. W. Hoffmann, Phys. Rev. C **31**, 538 (1985).

[8]M. V. Hynes, A. Picklesimer, P. C. Tandy, and R. M. Thaler,

Phys. Rev. Lett. **52**, 978 (1984); Phys. Rev. C **31**, 1435 (1985).
[9]J. A. McNeil, L. Ray, and S. J. Wallace, Phys. Rev. C **27**, 2123 (1983).
[10]M. L. Goldberger, M. T. Grisaru, S. W. MacDowell, and D. Y. Wong, Phys. Rev. **120**, 2250 (1960).
[11]D. Adams and M. Bleszynski, Phys. Lett. **136B**, 10 (1984).
[12]J. A. Tjon and S. J. Wallace, Phys. Rev. C **32**, 267 (1985); Phys. Rev. Lett. **54**, 1357 (1985).
[13]J. Fleischer and J. A. Tjon, Phys. Rev. D **21**, 87 (1980).
[14]C. Horowitz, Phys. Rev. C **31**, 1340 (1985).
[15]J. A. Tjon and S. J. Wallace, Phys. Rev. C **32**, 1667 (1985).
[16]J. A. Tjon and S. J. Wallace, Phys. Rev. C **35**, 280 (1987).
[17]A. Picklesimer and P. C. Tandy, Phys. Rev. C **34**, 1860 (1986).
[18]E. E. van Faassen and J. A. Tjon, Phys. Rev. C **28**, 2354 (1983).
[19]E. E. Van Faassen and J. A. Tjon, Phys. Rev. C **30**, 285 (1984).
[20]E. E. Van Faassen, Ph.D. thesis, University of Utrecht, 1985 (unpublished).
[21]C. Horowitz and B. D. Serot, Nucl. Phys. **A368**, 503 (1981).
[22]J. D. Bjorken and S. D. Drell, *Relativistic Quantum Mechanics* (McGraw-Hill, New York, 1964), p. 285.
[23]M. L. Goldberger and K. M. Watson, *Collision Theory* (Wiley, New York, 1964).
[24]A. Picklesimer, P. C. Tandy, R. M. Thaler, and D. Wolfe, Phys. Rev. C **29**, 1582 (1984).
[25]R. A. Arndt, L. D. Roper, R. A. Bryan, R. B. Clark, B. J. VerWest, and P. Signell, Phys. Rev. D **28**, 97 (1983).
[26]S. J. Wallace and J. L. Friar, Phys. Rev. C **29**, 956 (1984).
[27]S. J. Wallace, Ann. Phys. (N.Y.) **78**, 190 (1973).
[28]E. J. Stephenson, J. Phys. Soc. Jpn. (Suppl.) **55**, 316 (1985).
[29]P. Schwandt, private communication.
[30]A. Rahbar *et al.*, Phys. Rev. Lett. **47**, 1811 (1981).
[31]S. J. Wallace, in *Relativistic Dynamics and Quark-Nuclear Physics*, edited by M. B. Johnson and A. Picklesimer (Wiley, New York, 1986), p. 418.
[32]R. Machleidt, Ref. 28, p. 71.
[33]B. D. Serot and J. D. Walecka, Adv. Nucl. Phys. **16**, 1 (1986).
[34]M. R. Anastasio, L. S. Celenza, and C. M. Shakin, Phys. Rep. **100**, 327 (1983); L. S. Celenza and C. M. Shakin, *Relativistic Nuclear Physics* (World-Scientific, Singapore, 1986).
[35]R. Brockmann and R. Machleidt, Phys. Lett. **149B**, 283 (1984).